AN INVESTIGATION OF STRESS DISTRIBUTION IN A CATAMARAN CROSS-STRUCTURE

by

Charles Sidney Maclin

AN INVESTIGATION OF STRESS DISTRIBUTION IN A CATAMARAN CROSS-STRUCTURE

by

CHARLES SIDNEY MACLIN
Lieutenant, United States Navy

B.S., United States Naval Academy
(1963)

SUBMITTED IN PARTIAL FULFILLMENT OF THE
REQUIREMENTS FOR THE DEGREE OF
MASTER OF SCIENCE IN NAVAL ARCHITECTURE
AND MARINE ENGINEERING
AND THE PROFESSIONAL DEGREE OF
NAVAL ENGINEER

at the

MASSACHUSETTS INSTITUTE OF TECHNOLOGY

June, 1971

AN INVESTIGATION OF STRESS DISTRIBUTION IN A CATAMARAN CROSS-STRUCTURE

by

Charles Sidney Maclin
Lieutenant, United States Navy

Submitted to the Department of Naval Architecture and Marine Engineering on May 14, 1971, in partial fulfillment of the requirements for the Degree of Master of Science in Naval Architecture and Marine Engineering and the Professional Degree, Naval Engineer.

ABSTRACT

The objective of this thesis is to provide information regarding the distribution of transverse bending and shear stresses in a main transverse bulkhead of a catamaran cross-structure. Additionally, data is to be obtained on the width of deck plating between main bulkheads that resists transverse bending. The particular cross-structure configuration to be investigated is patterned after the United States Navy ASR-21 Class catamaran.

This study is of a two-dimensional nature to eliminate the influence of the adjacent transverse bulkheads on the stress distribution. In this configuration, the cross-structure bulkhead with its associated "effective breadth" of top and bottom deck plating resembles a large plate girder. The principle parameters varied are the breadth to depth (B/D) ratio of the cross-structure and the ratio of assumed total effective deck flange cross-sectional area to the cross-sectional area of the bulkhead web (A_f/A_w).

The photoelastic method of stress analysis employing a standard circular crossed polariscope in conjunction with a finite element computer program were used to conduct the investigation. The two-dimensional models were machined from Photolastic's PSM-1 material.

A total of twelve models were constructed using three values of B/D. Within each B/D series, the values of A_f/A_w were varied. The models were simply supported and loaded in vertical and horizontal directions. A finite element grid was established for each of the models and a series of computer calculations were made using the same loading and parameter variations as for the photoelastic models.

The stress distribution obtained with both methods of investigation indicates that the variation in transverse bending stress through the depth of the cross-structure is approximately linear for the vertical and horizontal loads acting separately. The shear stress (τ_{xy}) approximates a parabolic distribution for the same loads. Maximum shear stress (τ_{max}), however is nearly constant for the higher values of A_f/A_w. A value of A_f/A_w above which the level of stress no longer decreases for a given load was not determined. The data, however, suggests that such a value of A_f/A_w does exist. This data is valid in those areas away from the junction of hull and cross-structure. It is felt to be applicable to other catamaran cross-structures of similar design. The distribution of stress in the vicinity of the hull cross-structure junction is considered to be applicable to the ASR configuration only. The stress throughout the model resulting from the combined vertical and horizontal loads is not considered typical of that likely to be encountered in a prototype ship due to the proportionally excessive horizontal load required for photoelastic testing.

Three-dimensional studies should be undertaken with particular emphasis placed on the determination of the "effective breadth" of deck plating, and verification of the linearity of the transverse bending stress distribution through the depth of the cross-structure.

Thesis Supervisor: William M. Murray
Title: Professor of Mechanical Engineering

ACKNOWLEDGEMENTS

The author is sincerely grateful for the suggestions and guidance received throughout the investigation from Professor William M. Murray, Department of Mechanical Engineering. He wishes to acknowledge too, the advice and assistance provided by Professor Alaa Mansour, Department of Naval Architecture and Marine Engineering.

Special appreciation is extended to Mr. John B. O'Brien of the Naval Ship Engineering Center and to Dr. John C. Adamchak of the Naval Ship Research and Development Center for providing assistance and background information essential to the completion of this thesis.

TABLE OF CONTENTS

TABLE OF CONTENTS
(Cont'd)

LIST OF FIGURES

LIST OF FIGURES
(Cont'd)

LIST OF TABLES

INTRODUCTION

As a distinctive ship form, catamarans have been in existence for several hundred years. The Polynesians were perhaps the first to use the catamaran in the form of their outrigger canoes. More recently, the E. W. THORNTON and RIDGELY WARFIELD have been built in the United States for offshore drilling and oceanographic work respectively. With the development of the submarine rescue ship (ASR 21 Class) as a catamaran, the U. S. Navy became interested in this type of hull form.

Prior to the developments indicated above, the catamaran was regarded primarily as a novelty ship, with little or no investigation of the stress distribution in the cross-structure having been performed. This lack of information was pointed out by Lankford in his article on the structural design of the ASR catamaran (Reference 9).

In his article, Lankford indicated three primary areas that required investigation in order to properly design the cross-structure of the ASR. These areas included:

(a) Type of loading imposed on the hulls that would be critical to cross-structure design.

(b) Distribution of the loads within the cross-structure joining the two hulls.

(c) Design of the joint between the cross-structure and the hulls to withstand the loading imposed on it.

For the ASR, statistical analysis of wave data was used to determine the critical loading. The transverse bulkheads between the two hulls together with an effective breadth of plating as the upper and lower flanges were considered to be the primary load bearing members of the cross-structure. The bottom plating of the cross-structure was "dove-tailed" into the hulls to form the joint between hull and cross-structure.

The objective of this thesis was formulated from (b) above. The experimental work in the thesis was undertaken to provide information regarding the distribution of transverse bending and shear stresses within a main transverse bulkhead of the cross-structure along with data on the width of plating between the main bulkheads that resists transverse bending.

Due to the inherent complexity of the problem, it was decided to conduct this initial investigation utilizing two dimensional techniques. The method of investigation would include the use of photoelastic models and a finite element computer program, FINEL, provided by the Naval Ship Research and Development Center, Washington, D.C.

A series of twelve bulkhead models were constructed from photoelastic plastic (PSM-1). The models were scaled to the outline of ASR Bulkhead #84. The model parameters varied were the breadth to depth ratio of the cross-structure, B/D, and the ratio of the cross-sectional areas of the deck flanges to the bulkhead web, A_f/A_w. These parameters are

illustrated in Figure I, and listed in Table B-1. Additionally, these same models were used for the basis for the computer models. Loading was applied to simulate simple bending of the cross-structure from vertical and horizontal loads.

No doubt this procedure is an oversimplification of the actual situation. However, in order to gain an insight into the problem and obtain some information in the short time available, it was considered acceptable. To my knowledge, there has not been a similar investigation conducted in this area.

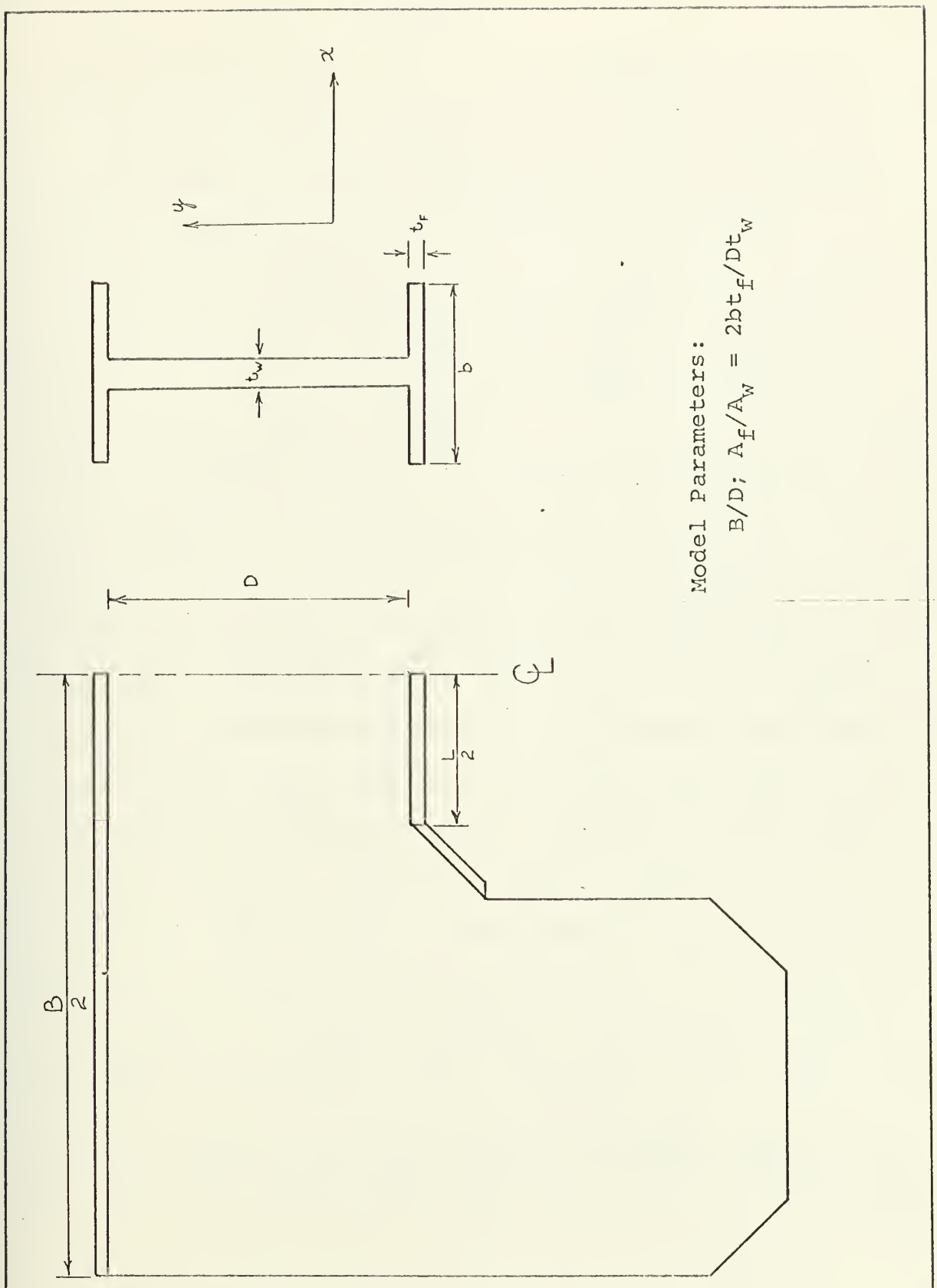

FIGURE I
MODEL CONFIGURATION AND PARAMETERS

PROCEDURE

As previously stated, the primary objectives of this thesis were to obtain an insight into the distribution of transverse bending and shear stresses in a main transverse bulkhead of a catamaran cross-structure, and to gather data on the amount of plating between bulkheads that resist such bending stresses. The objectives were accomplished through the use of two-dimensional photoelastic models and a finite element computer program.

The photoelastic models were prepared from PSM-1. Complete details as to model preparation are contained in Appendix B. The polariscope in the Ship Structures Laboratory was set up and aligned to give a dark field presentation. The models were placed in the loading frame and a load of 200 psi was applied to the loading ram head.* The models were simply supported and loaded separately in horizontal and vertical directions. Figure II depicts the loading of the models. The same load was applied to all models at the same location. There were no supports or clamps used to prevent out-of-plane bending of the models. With the models in a loaded condition, photographs of the fringe patterns were made using a Polaroid 4" x 5" film

*A load of 200 psi on the ram head has no significance other than this load provided good fringe pattern photographs.

holder and Polaroid Type 52 film. Using these photographs, the frings orders at several points were determined. Complete details of these procedures are contained in Appendix B. The fringe pattern photographs are included in Appendix D, while the fringe order data is presented in Appendix C.

In conjunction with the photoelastic testing, a finite element grid was established for each model. Ideally, the fringe pattern photographs should be used to identify those areas of high stress concentration so that a finer mesh grid can be used in these areas. Due to the shortage of time, and the desire to compare the two methods of investigation, a grid was established early so that it might be scribed on the plastic models. Anticipating an area of stress concentration at the joining of hull and cross-structure, the grid was made finer in this region.

The finite element grid was next transformed into the appropriate format in accordance with Reference 14. Computer runs were made for each of the models. Each computer model was loaded at the same location and with the same load as the corresponding photoelastic model. Additionally, results were obtained with a combined vertical and horizontal load. The results were then interpreted as outlined in Appendix C. Additional information on the finite element method is contained in Appendices A and B, while a summary of the computer results is contained in Appendix C.

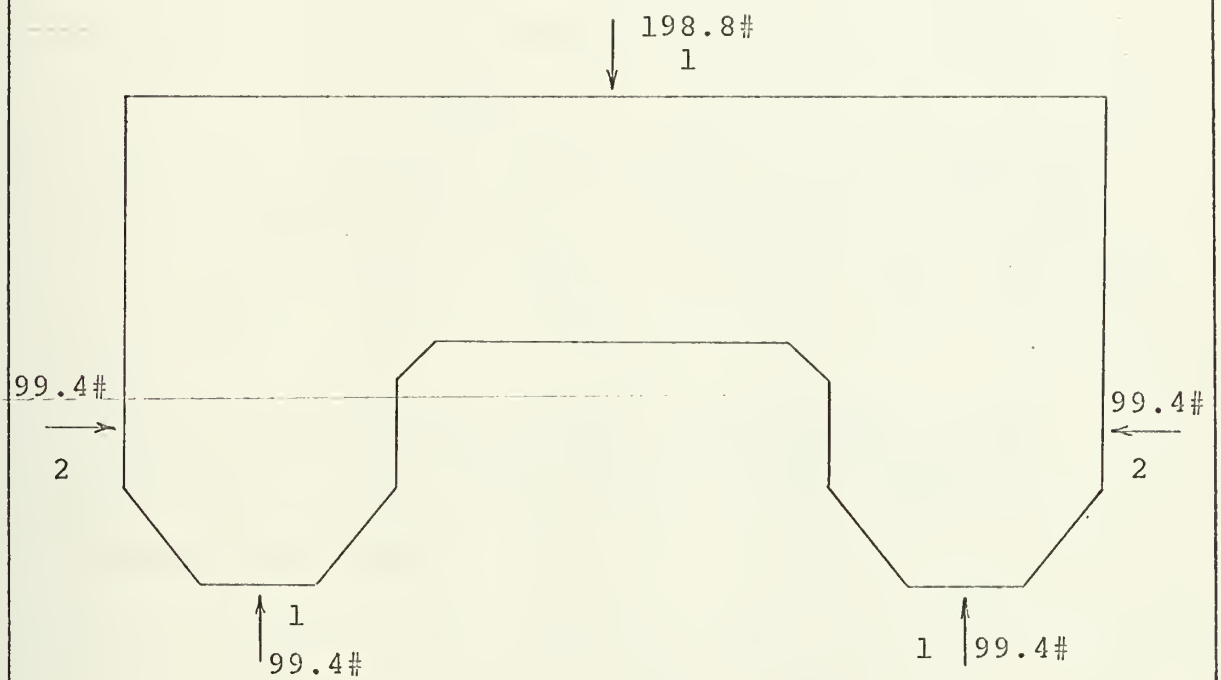

Load 1: 1 only

Load 2: 2 only

Load 3: 1 and 2 (Computer only)

FIGURE II
MODEL LOADING

RESULTS

1. Isochromatic fringe patterns for all model loadings are shown in Figures D-2 through D-13.
2. Tabulated computer results for all model loadings are presented in Tables C-1 through C-9.
3. The effect of varying B/D and A_f/A_w on the transverse bending stress at the junction of cross-structure and hull is shown in Figures III, IV, V, VI, VII, and VIII.
4. The effect of varying B/D and A_f/A_w on the transverse bending stress at a point on the bottom of the cross-structure is shown in Figures IX, X, XI, XII, XIII, and XIV.
5. Typical vertical shear stress distribution in the cross-structure at the junction of hull and cross-structure is shown:
   (a) in Figure XV for vertical loads
   (b) in Figure XVI for horizontal loads
   (c) in Figure XVII for combined loads.
6. Typical vertical shear stress distribution in the cross-structure at a distance $x/L = 1/3$ from the model centerline is shown in Figure XVIII.
7. Transverse bending stress distribution in the cross-structure at the junction of hull and cross-structure for the unstiffened models is shown in Figure XIX.

8. Typical transverse bending stress distribution in the cross-structure at the junction of hull and cross-structure for varying degrees of model stiffening is shown in Figure XX.

9. Transverse bending stress distribution in the cross-structure for unstiffened models at a distance of $x/L = 1/3$ from the model centerline is shown in Figure XXI.

10. Typical transverse bending stress distribution in the cross-structure at a distance of $x/L = 1/3$ from the model centerline for varying degrees of model stiffening is shown in Figure XXII.

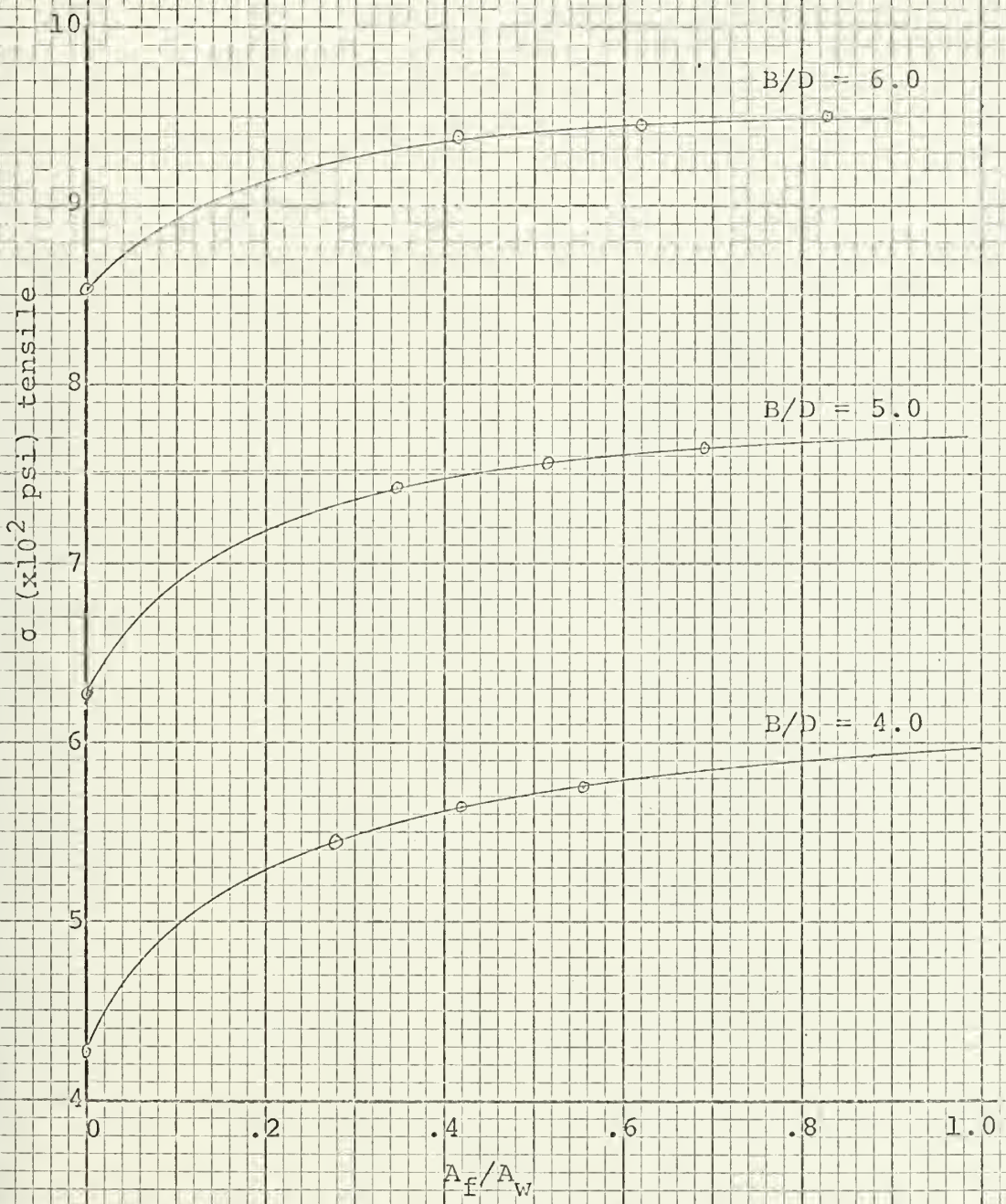

FIGURE III
TRANSVERSE BENDING STRESS AT JUNCTION
VERTICAL LOAD

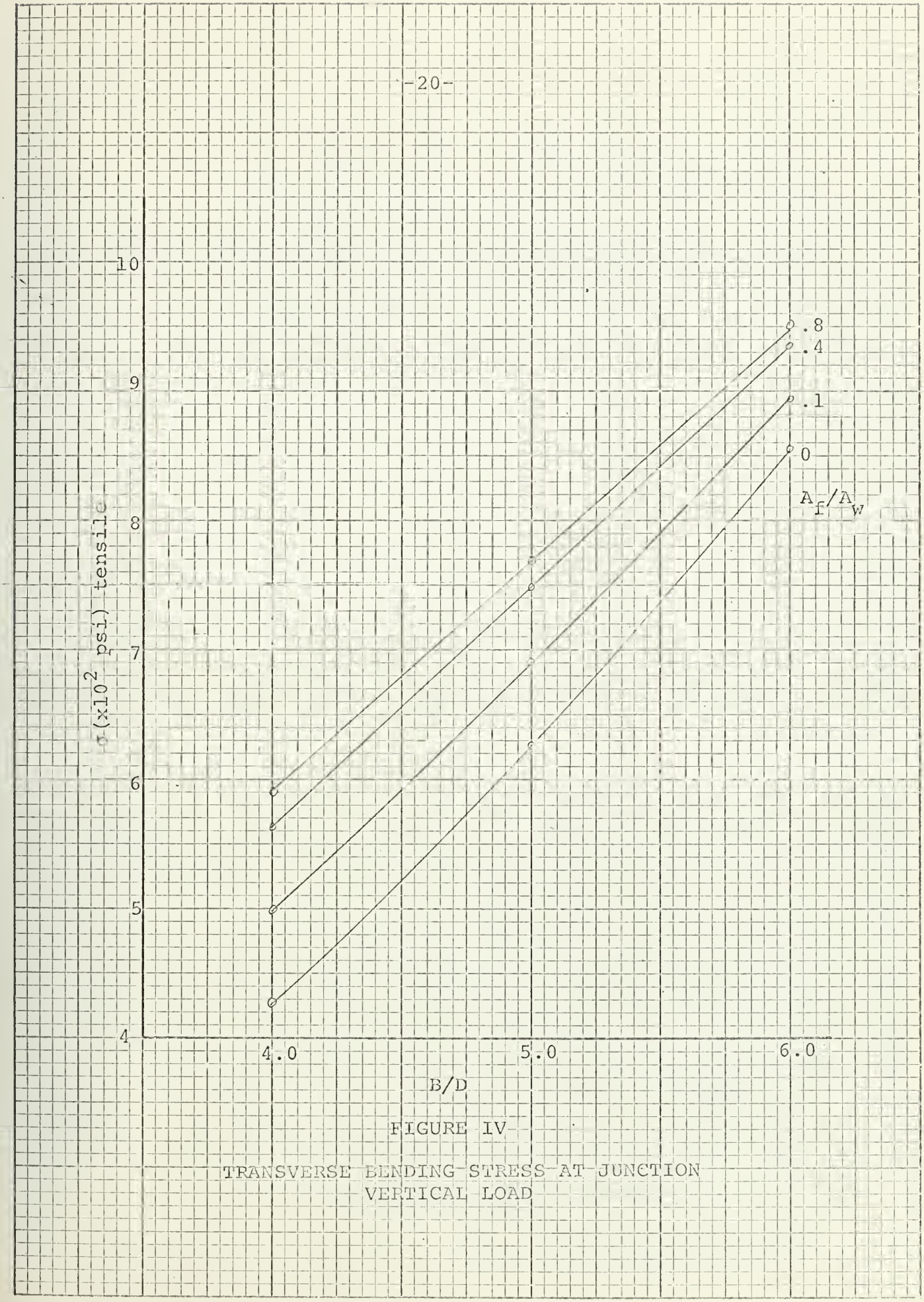

FIGURE IV

TRANSVERSE BENDING STRESS AT JUNCTION
VERTICAL LOAD

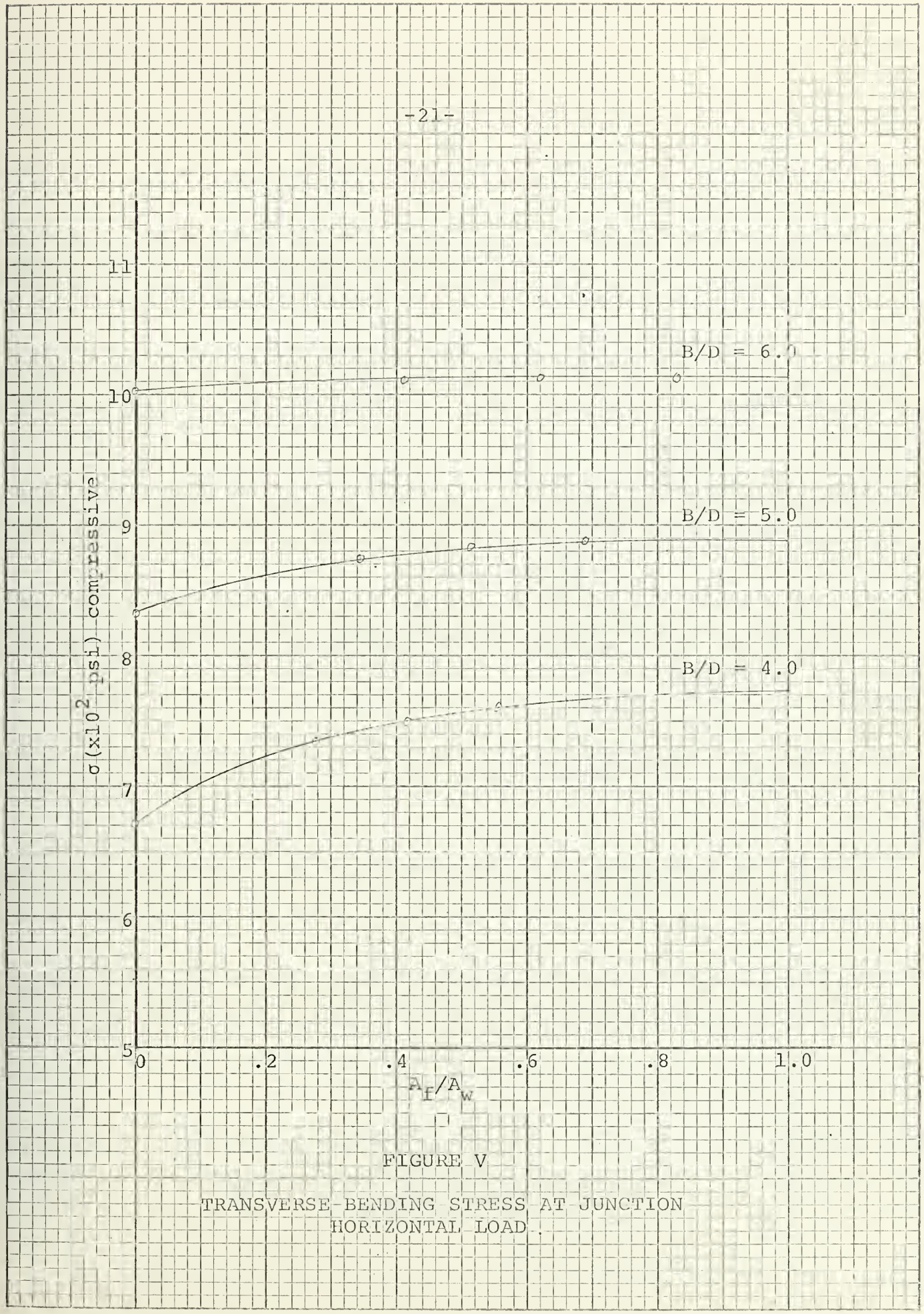

FIGURE V

TRANSVERSE BENDING STRESS AT JUNCTION
HORIZONTAL LOAD

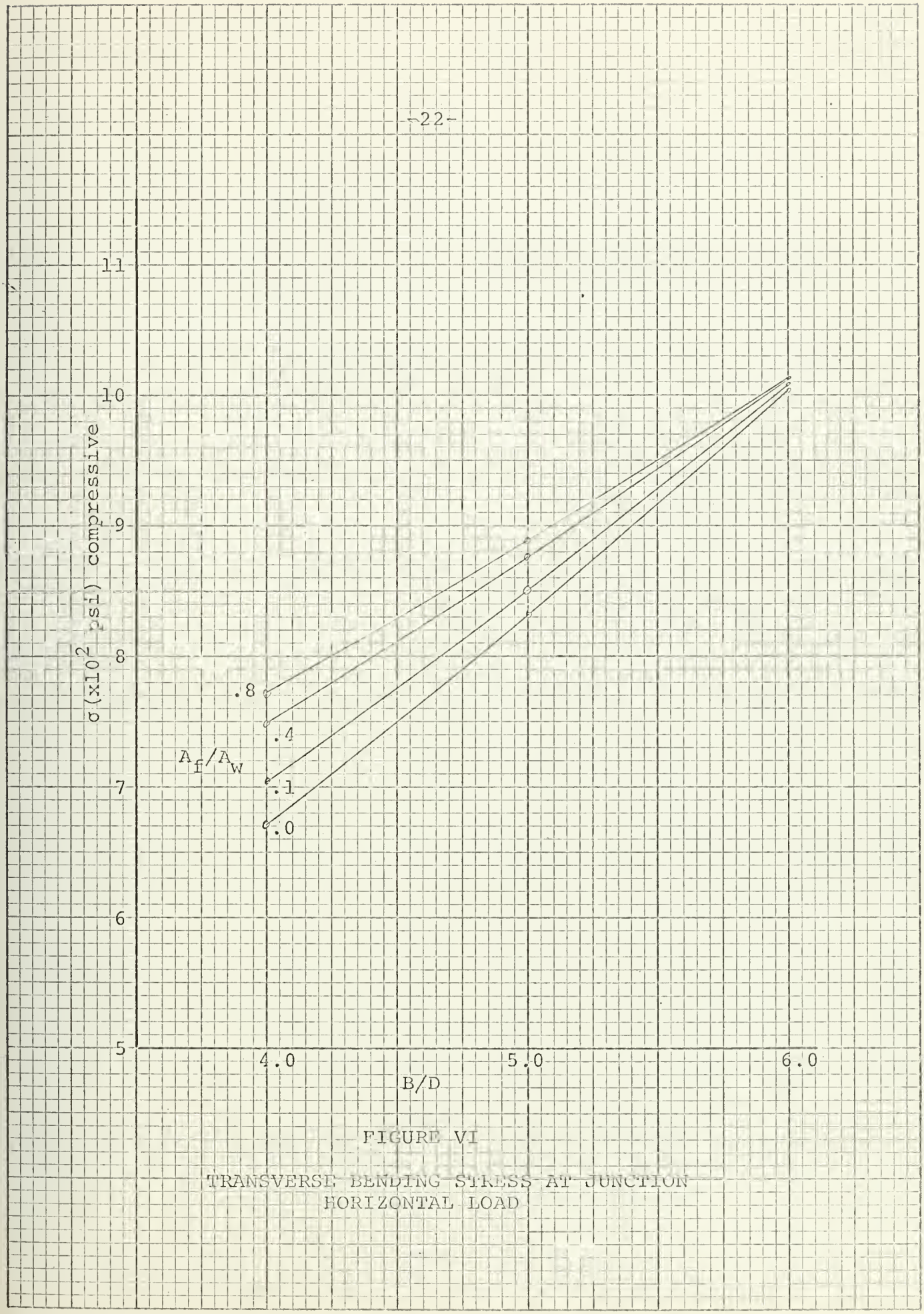

FIGURE VI

TRANSVERSE BENDING STRESS AT JUNCTION
HORIZONTAL LOAD

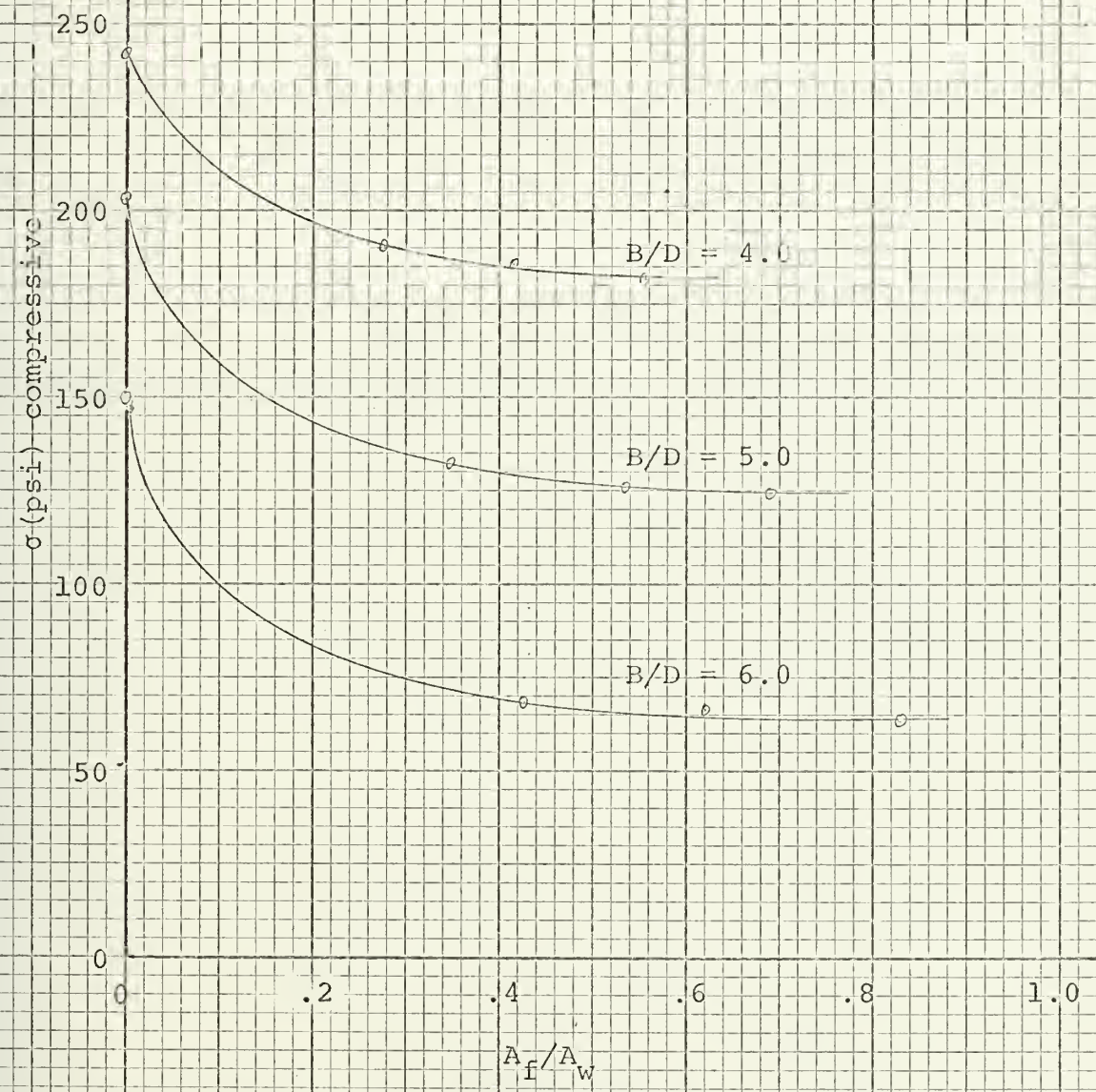

FIGURE VII
TRANSVERSE BENDING STRESS AT JUNCTION
COMBINED LOAD

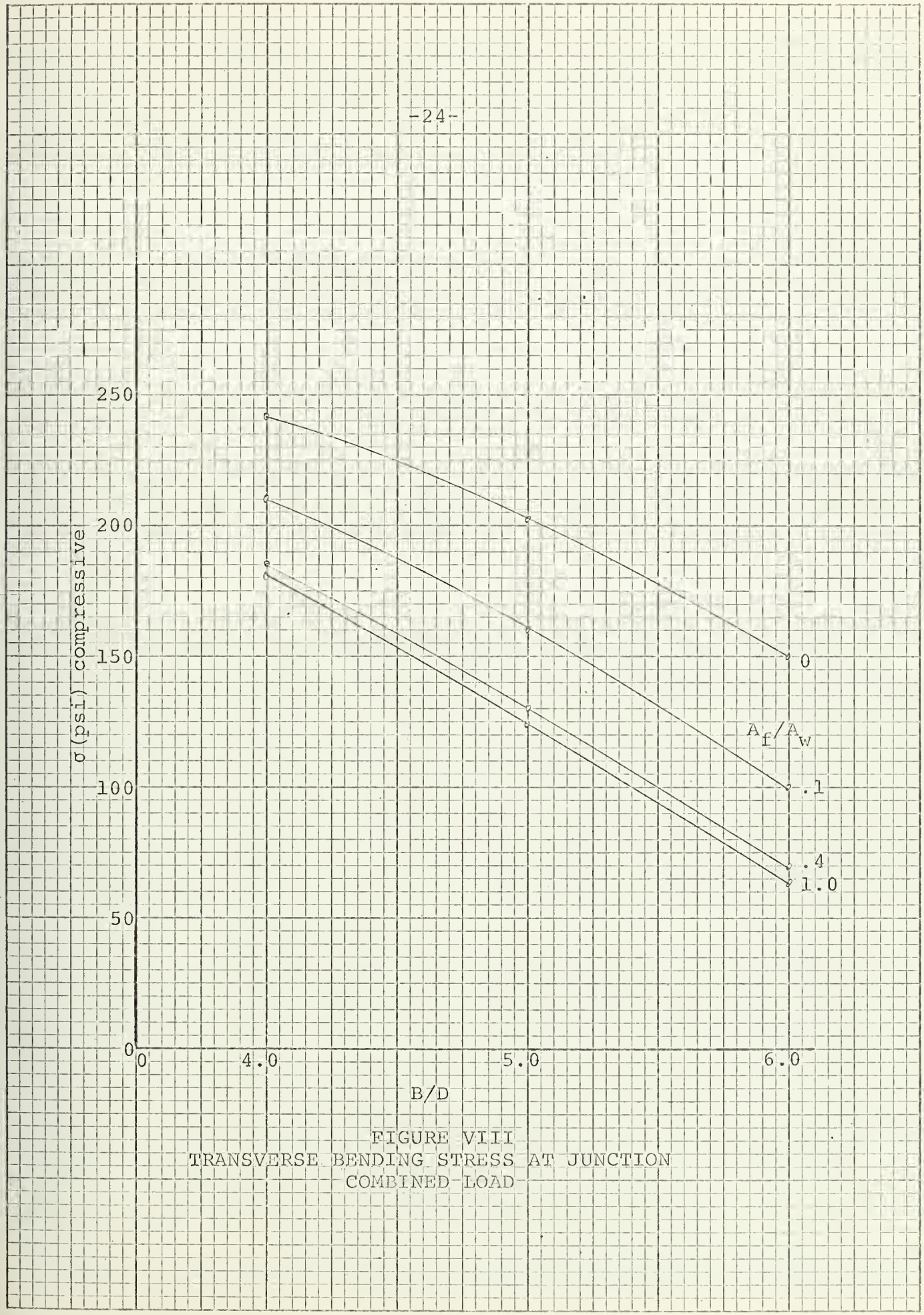

FIGURE VIII
TRANSVERSE BENDING STRESS AT JUNCTION
COMBINED LOAD

FIGURE IX
TRANSVERSE BENDING STRESS AT x/L = 1/3
VERTICAL LOAD

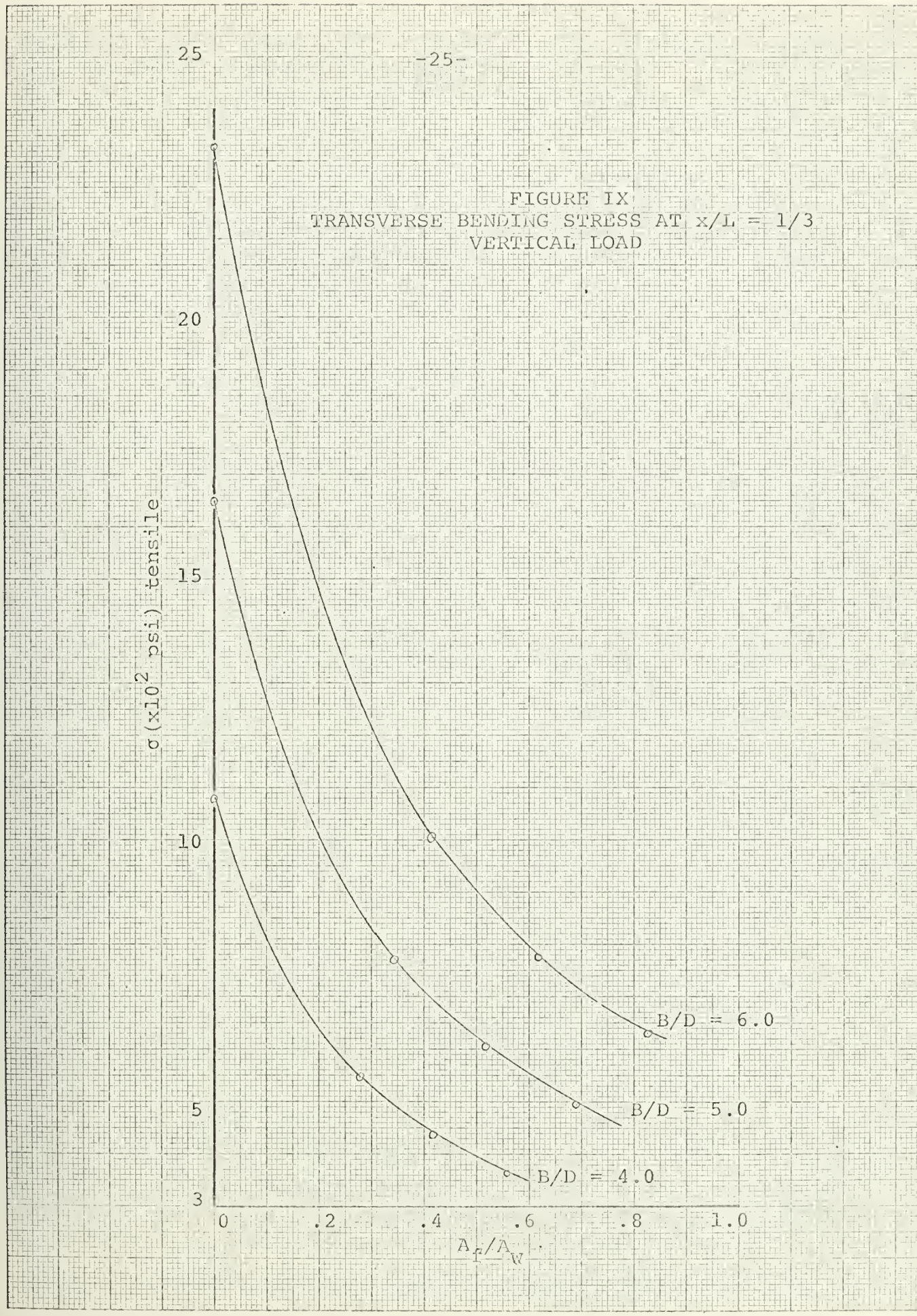

FIGURE X
TRANSVERSE BENDING STRESS
AT x/L = 1/3
VERTICAL LOAD

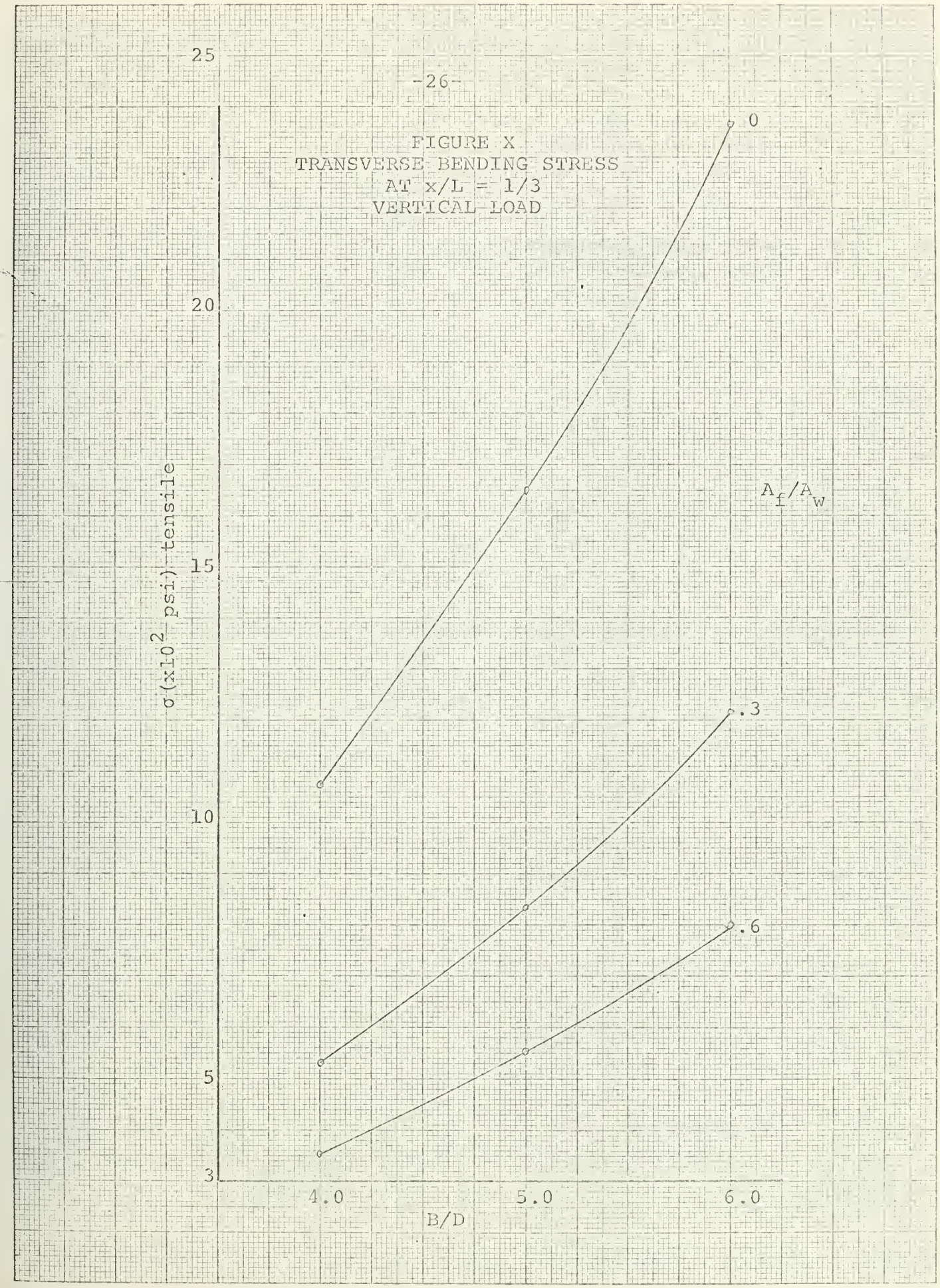

FIGURE XI

TRANSVERSE BENDING STRESS
AT x/L = 1/3
HORIZONTAL LOAD

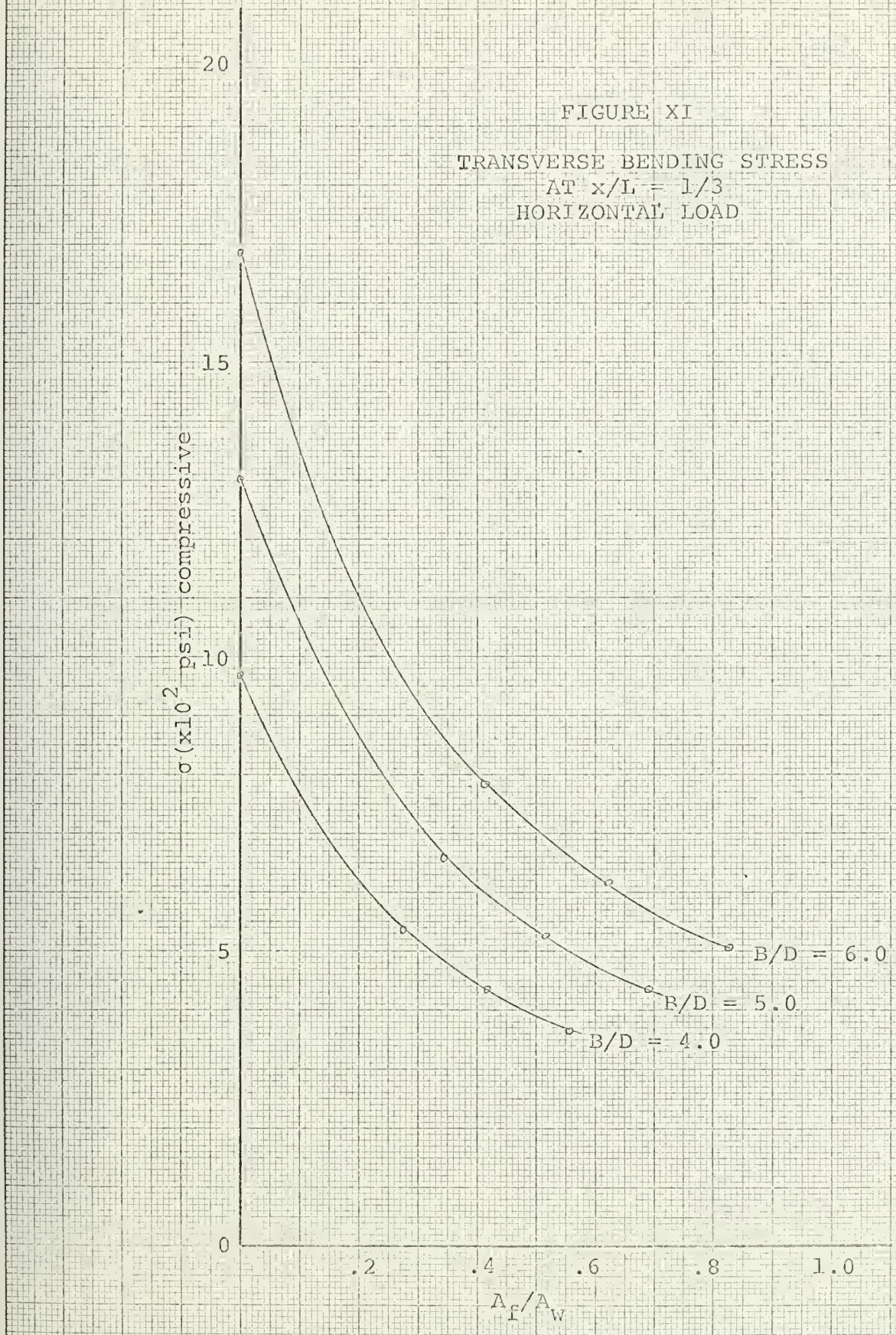

FIGURE XII

TRANSVERSE BENDING STRESS AT x/L = 1/3
HORIZONTAL LOAD

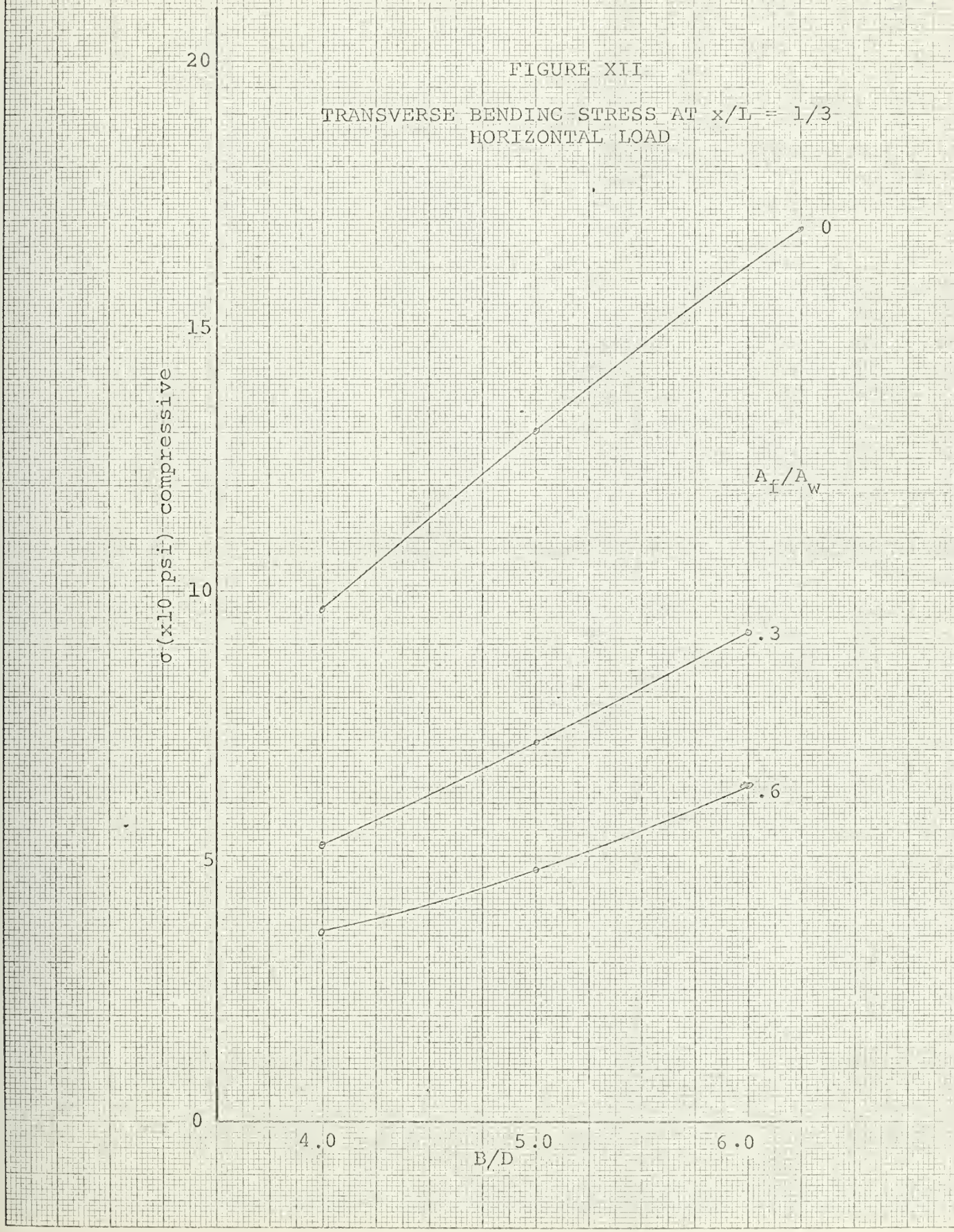

FIGURE XIII

TRANSVERSE BENDING STRESS AT x/L = 1/3
COMBINED LOAD

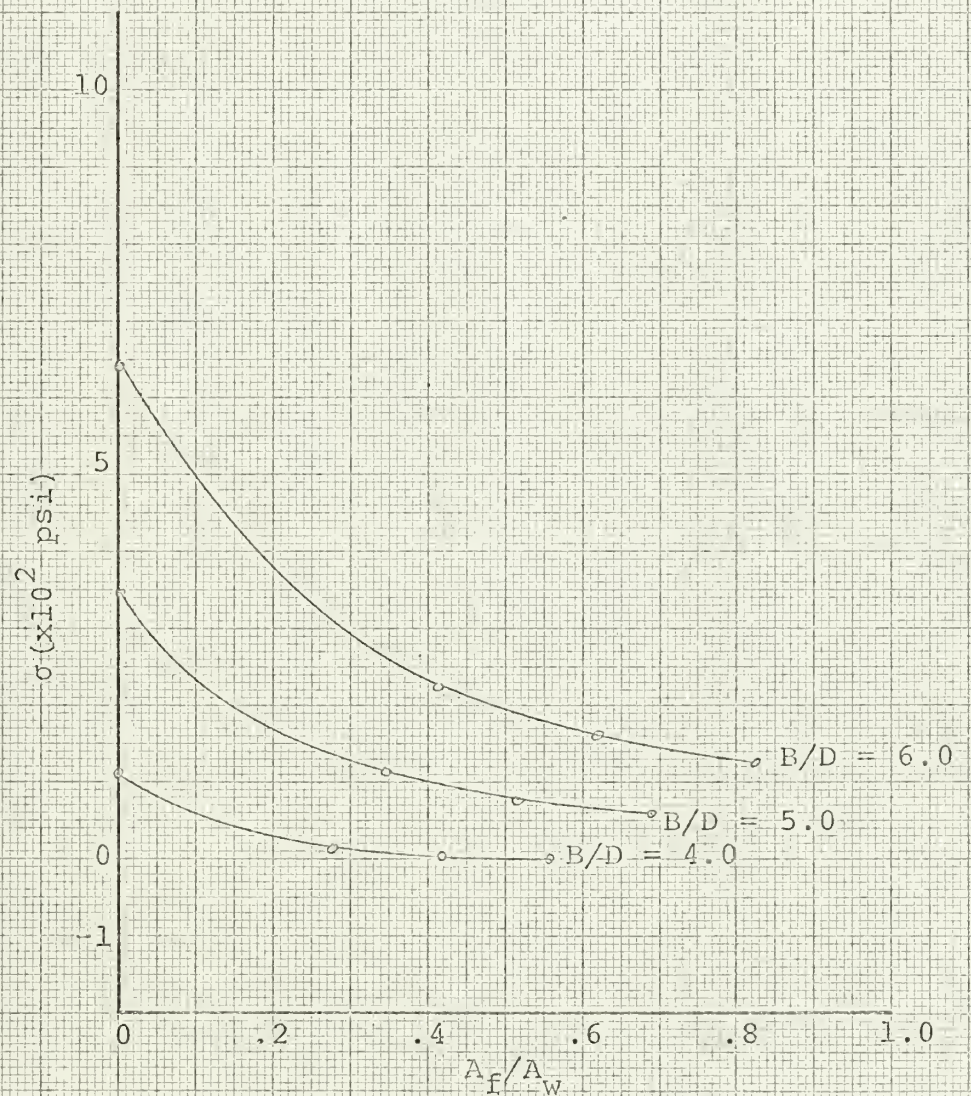

FIGURE XIV

TRANSVERSE BENDING STRESS AT x/L = 1/3
COMBINED LOAD

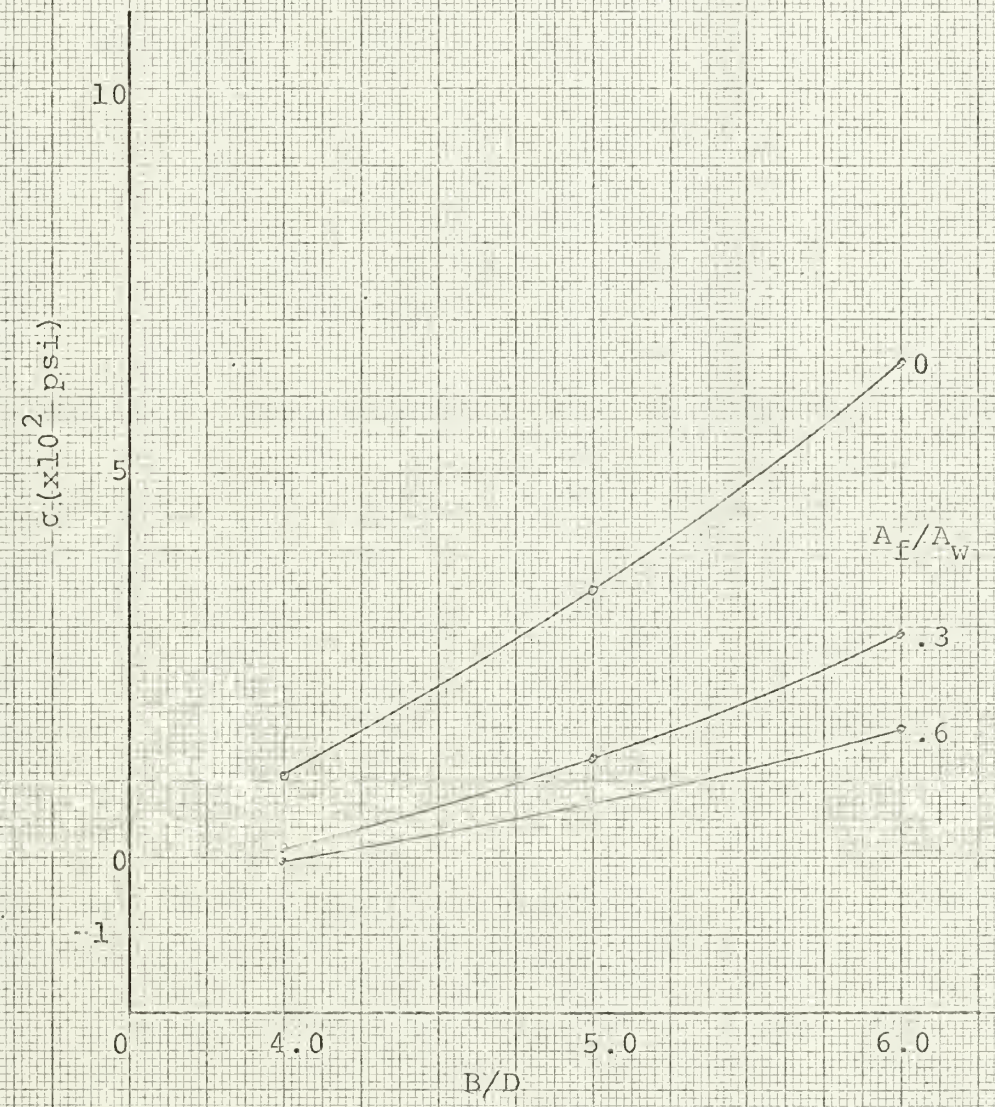

FIGURE XV

SHEAR STRESS AT JUNCTION
VERTICAL LOAD
B/D = 4.0

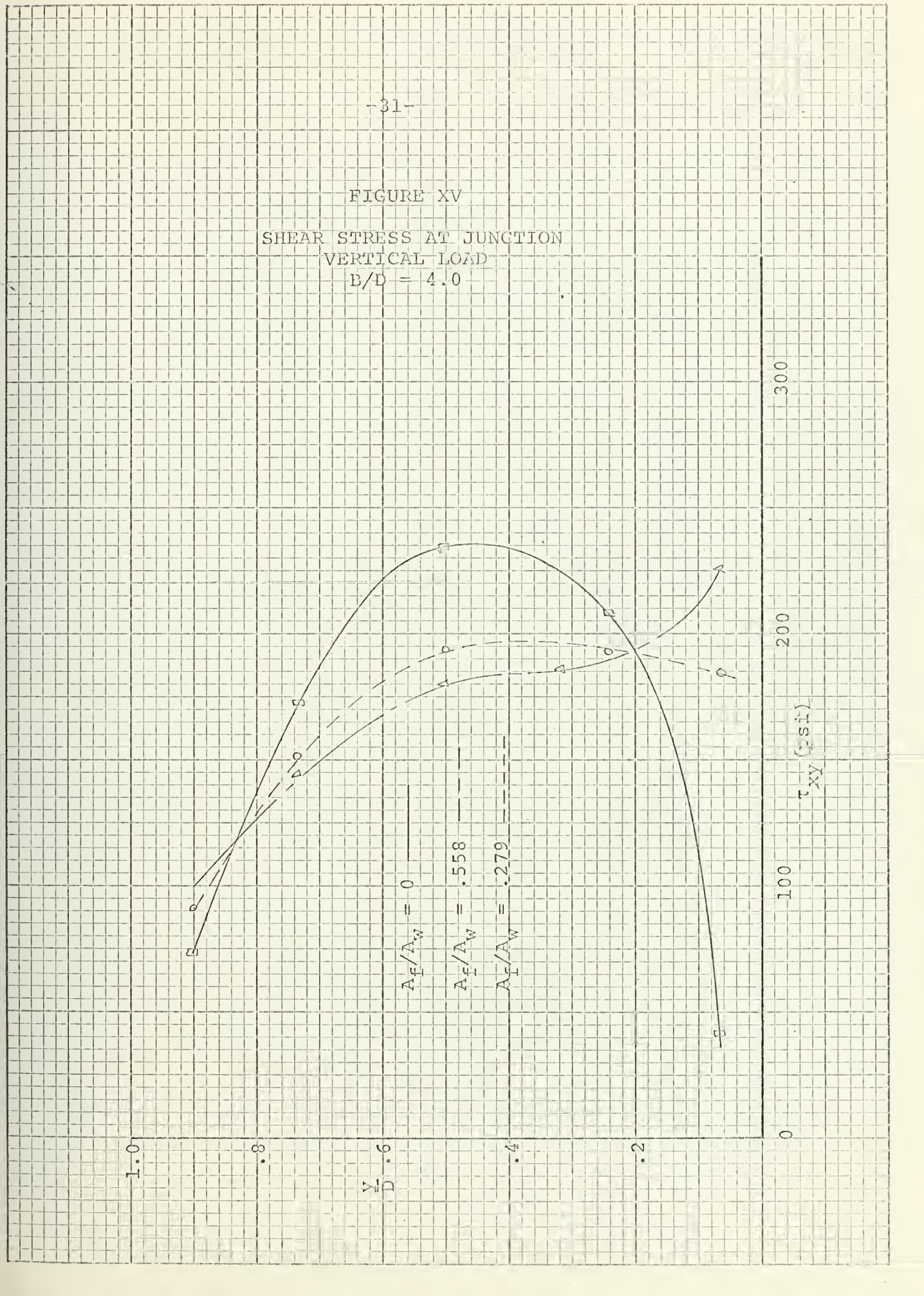

FIGURE XVI

SHEAR STRESS AT JUNCTION
HORIZONTAL LOAD
B/D = 5.0

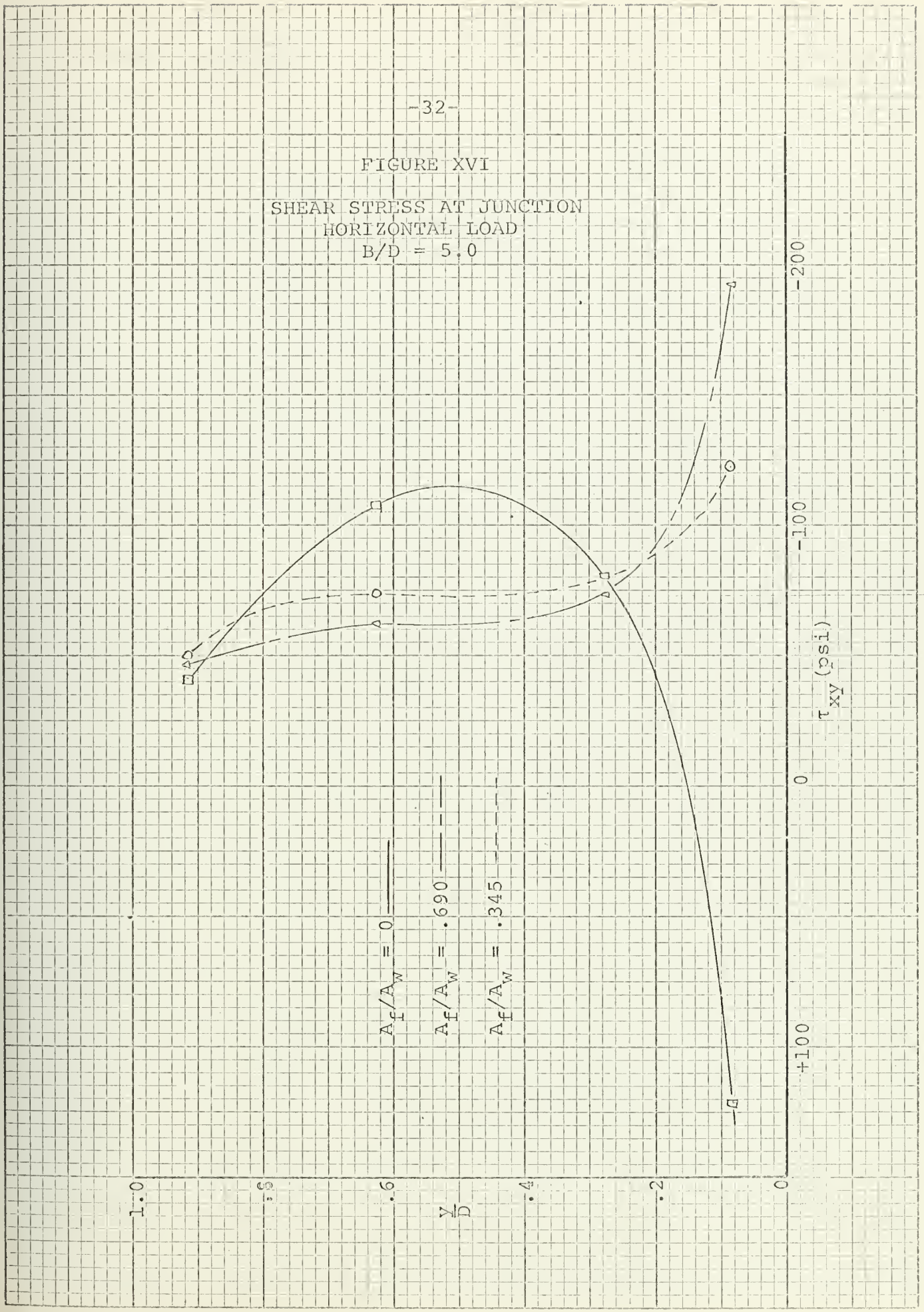

FIGURE XVII

SHEAR-STRESS AT JUNCTION
COMBINED LOAD
B/D = 6.0

FIGURE XVIII

SHEAR STRESS AT x/L = 1/3
VERTICAL LOAD
B/D = 5.0

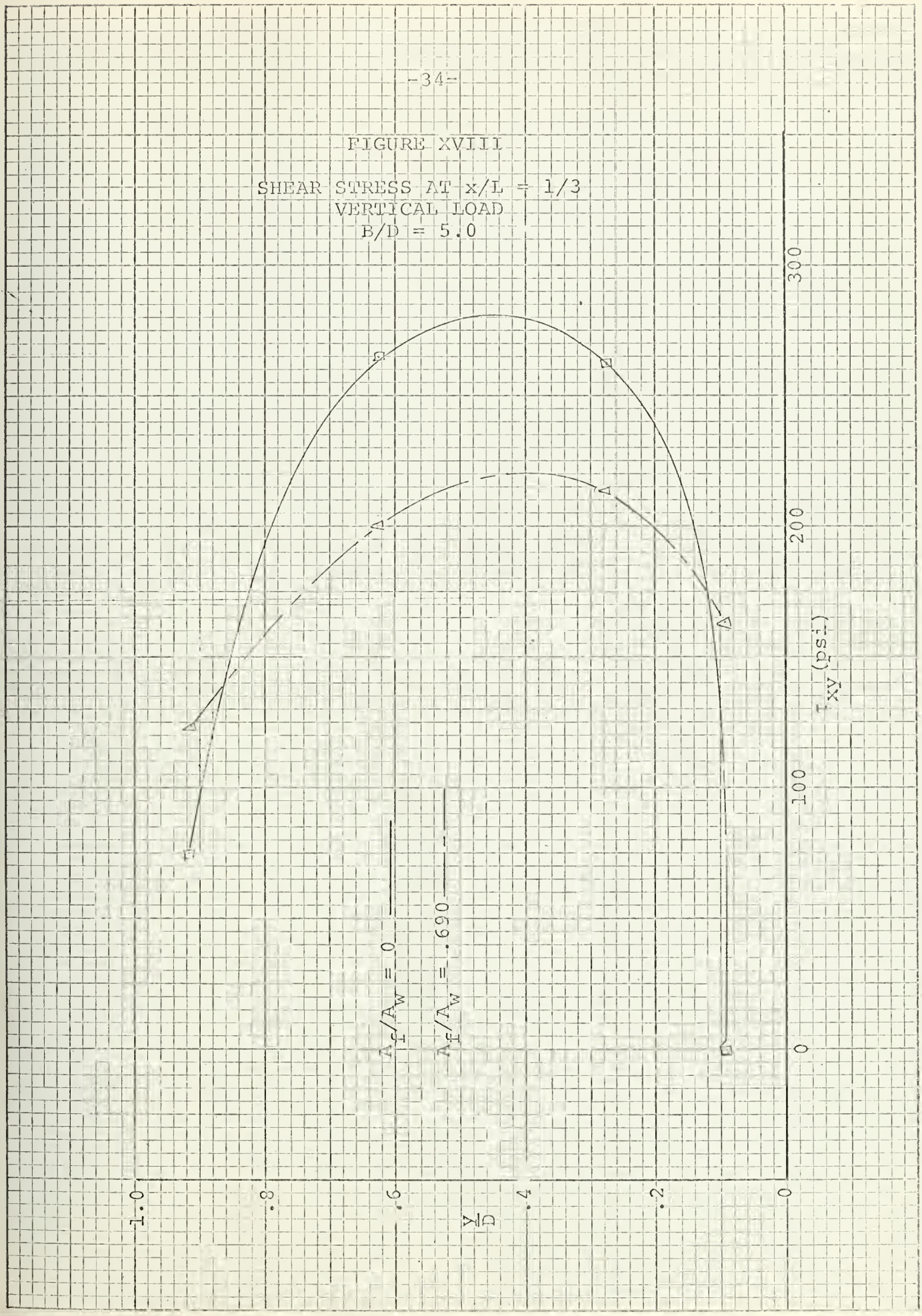

FIGURE XIX

TRANSVERSE STRESS DISTRIBUTION AT JUNCTION
VERTICAL LOAD
$A_f/A_w = 0$

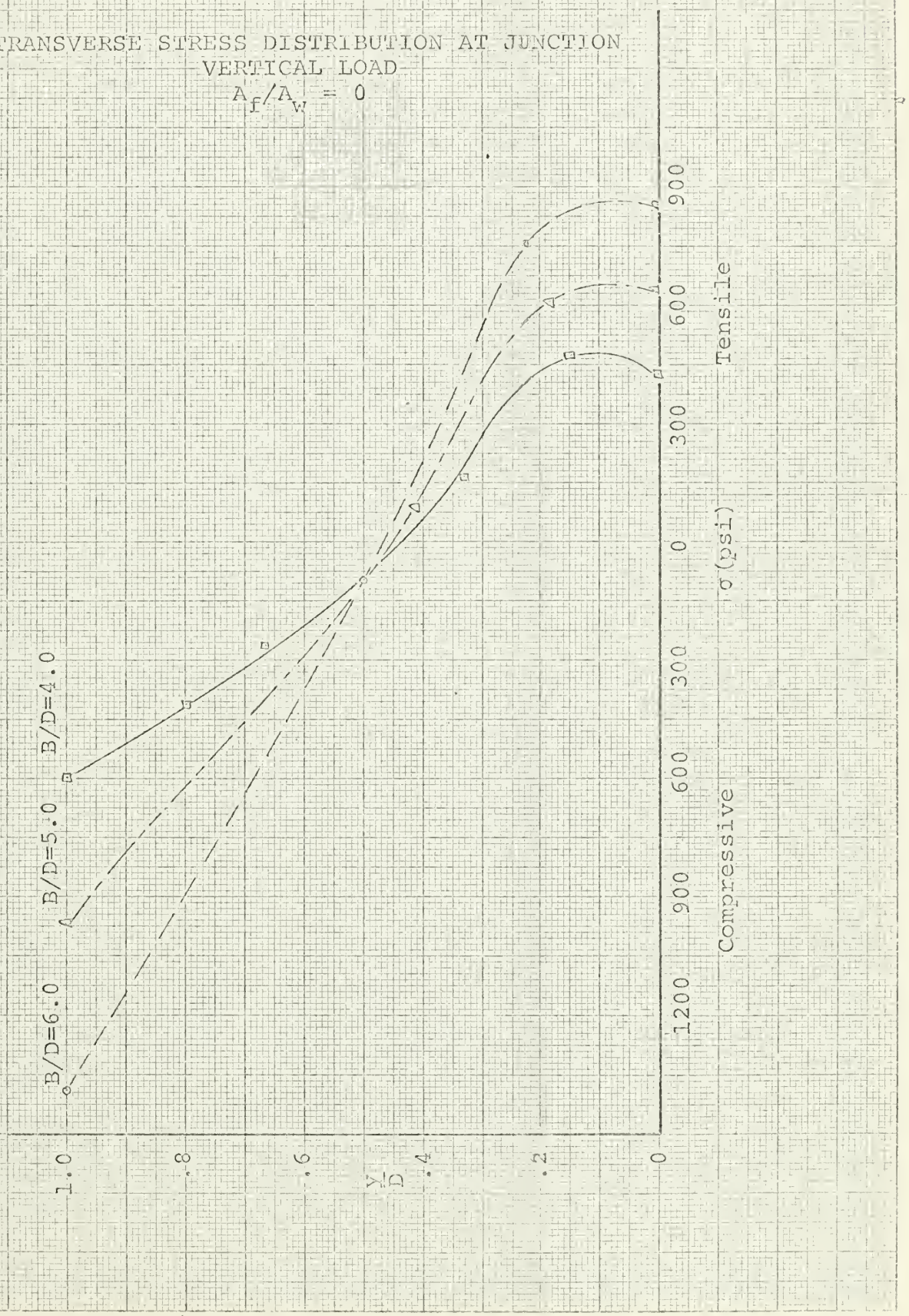

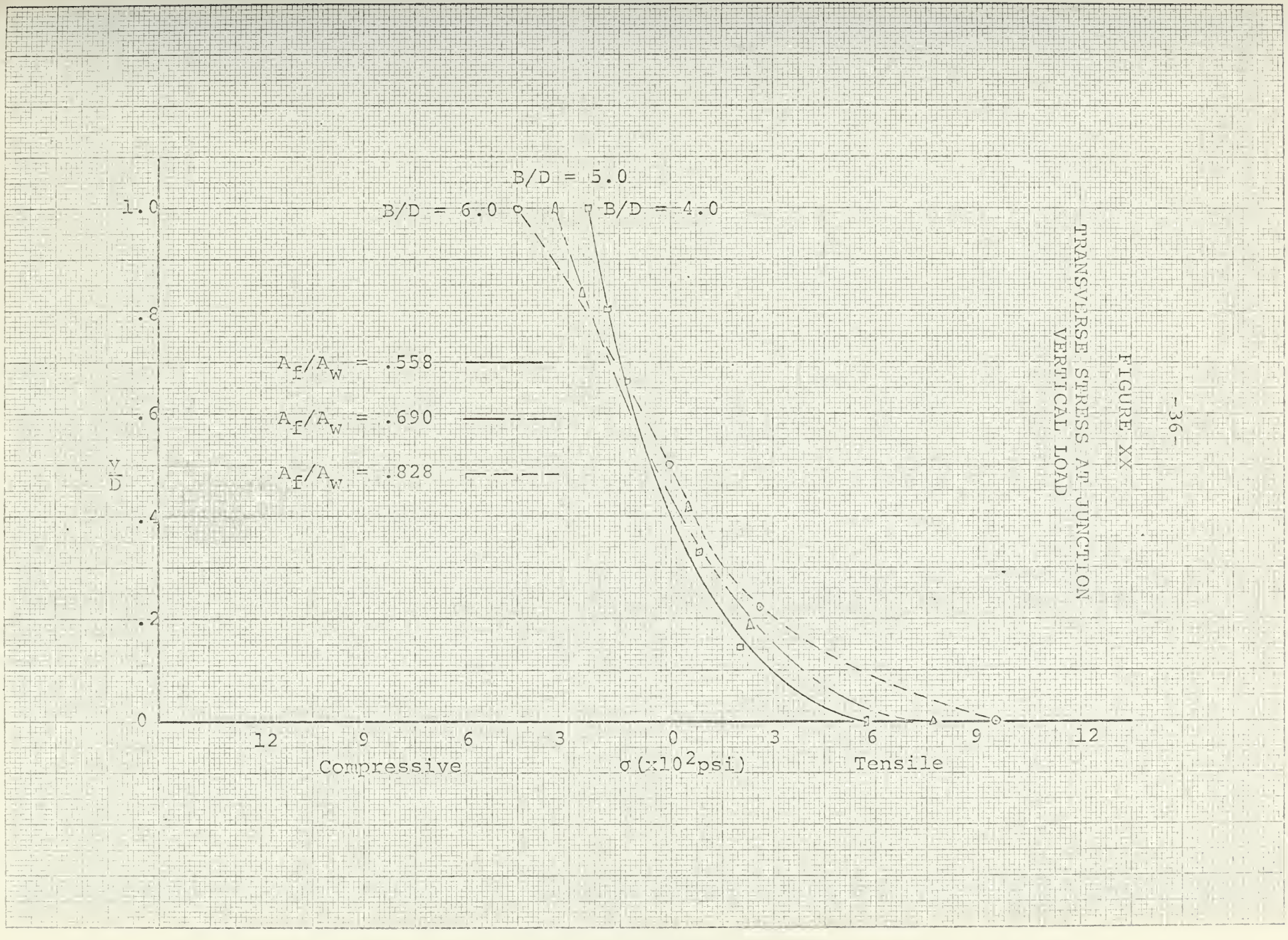

FIGURE XX

TRANSVERSE STRESS AT JUNCTION
VERTICAL LOAD

FIGURE XXI

TRANSVERSE STRESS AT x/L = 1/3
VERTICAL LOAD
$A_f/A_w = 0$

FIGURE XXII

TRANSVERSE STRESS DISTRIBUTION AT x/L = 1/3
VERTICAL LOAD

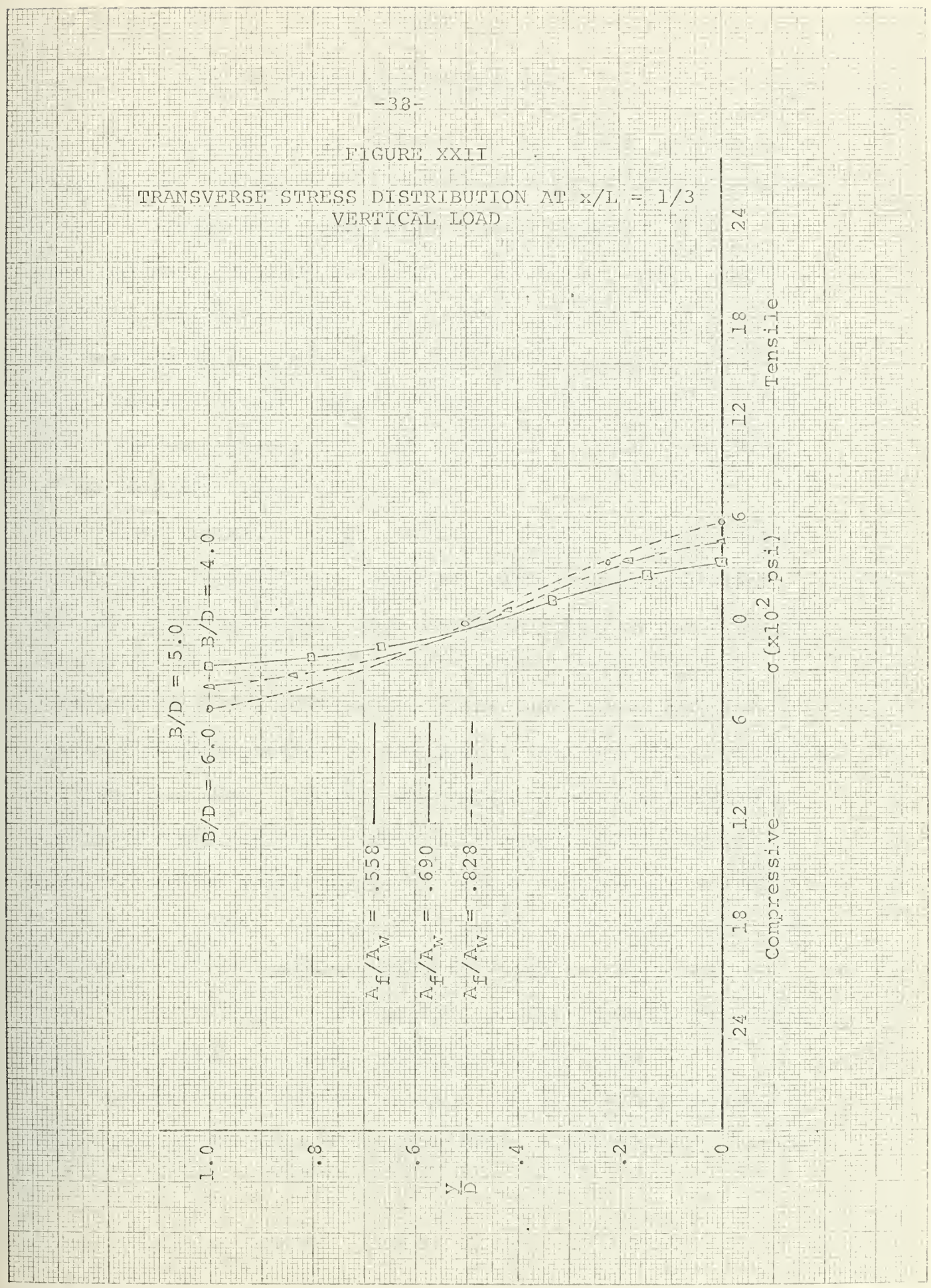

DISCUSSION OF RESULTS

Isochromatic fringe patterns of horizontal and vertical loadings were obtained for each of the model configurations listed in Table B-1. Additional fringe patterns were obtained for models 2, 3, 4, 6, 7, 8, 10, 11, and 12 with only the top "deck flange" in place. All fringe patterns are reproduced in Appendix D. The fringe patterns are of only one-half of the model. However, since the models and the loads are symmetrical, the patterns are representative of the overall stress distribution.

Unfortunately, the photoelastic results of this thesis are largely qualitative. Monetary restrictions prevented the use of an additional less sensitive material in order to obtain the directions of the isoclinics. Photographic equipment size limitations prevented the photographing of the entire half portion of the model. Without the isoclinics and edge stresses, the only quantitative results obtainable are the differences in principle stresses and the distribution of maximum shear stresses. These results are valuable in their own right. However, for purposes of comparison with the format of the computer results, they are difficult to use. It is felt that the addition of the lines of principle stress would be a valuable addition to the data.

The amount of computer output for each model loading is quite extensive. It was not possible to include all of this

raw data; however, those stresses thought to be particularly relevant are included in Appendix C. The values for the stress distribution plots in the previous section were obtained from the computer data.

Figures III through VIII show the stress value at the junction of the hull and cross-structure for all models for all types of loading. For the horizontal and vertical loads acting separately these graphs indicate that increasing either B/D or A_f/A_w results in an increased level of stress at the junction, the stress being tensile for vertical loading and compressive for horizontal loads. This trend is confirmed by the fringe pattern photographs. Additionally, these figures suggest that there is a limiting value of A_f/A_w with increasing B/D. Figures VII and VIII, which are for combined loading, are interesting in that they indicate a significant drop in the stress at the junction with increasing B/D and A_f/A_w . These curves are only of significance however for this type of joint design. Further, the load in the horizontal direction is felt to be excessive, it being improbably that the prototype catamaran would experience a load of such a relatively large magnitude. For these reasons, it is doubtful that such a significant reduction of stress would occur in the prototype.

Figures IX through XIV illustrate the varying of the same model parameters as above; however, the point of interest is now towards the model centerline away from the

junction of the cross-structure and hulls. The results are as might be expected, that stress level decreases with decreasing B/D and increasing A_f/A_w. Unfortunately, this set of model parameters did not establish that point at which A_f/A_w is no longer effective in reducing the stress level. The trends of these curves can readily be seen in the fringe pattern photographs, with the effect of increasing A_f/A_w dramatically illustrated. No doubt the configuration of the hull cross-structure junction has some influence on these curves. However, it is doubtful that the influence would be so great as to prevent these curves being applicable to a catamaran of the same general cross-structure design.

Figures XV and XVII are representative of the shear stress distribution at the hull cross-structure junction of the various models and loadings. The results of all models are not plotted because all of the curves are of the same general shape. For the horizontal and vertical loads on the unstiffened models the stress distribution is of the expected parabolic shape. However, the results for the stiffened models depart radically from this shape in the region of the "notch." For the combined load, the curves are back to the parabolic type. The same remarks regarding the applicability of these curves may be made as previously; namely that the curves should not be applied directly to other hull cross-structure junction designs.

Figure XVIII is representative of the shear stress distribution at points other than along the hull cross-structure junction line. Generally, the shear stress (τ_{xy}) increases with increasing B/D and decreasing A_f/A_w. The photoelastic fringe patterns indicate that maximum shear stress (τ_{max}) curves have opposite curvature to that shown in Figure XVIII, the maximum shear occurring along the top and bottom of the cross-structure. For the vertical loads, the fringe patterns also show that τ_{max} is nearly constant through the depth of the cross-structure. This latter result is most applicable to those models with higher value of A_f/A_w.

The effect of the junction on the transverse bending stress due to vertical loads is shown quite clearly in Figure XIX, while Figure XX indicates the additional effect of stiffening at the junction. The amount of stress reduction at the top of the cross-structure is also quite evident. Again, these curves are representative for all models tested.

The final two figures, XXI and XXII are representative of the transverse bending stress distribution due to vertical loads, away from the hull cross-structure junction. The form of the curves for the unstiffened models compares favorably with that for deep beam theory with D/L ratio equal to 1/2. However, the stiffened model results do not exhibit this trend. The curves in Figures XXI and XXII can very nearly

be approximated by straight lines, thereby suggesting that the stress distribution is more like that predicted by standard beam theory, rather than plate or deep beam theory. Should this be true, significant savings in steel weight could be achieved in the full sized ship structure.

Comparison of the photoelastic method of stress analysis with analysis utilizing the computer is difficult in that sufficient comparable numeric data is not available. Comparison of the edge stresses predicted by the computer and those calculated from the photoelastic models agree within about six percent. The value of the photoelastic models in presenting the overall picture of stress distribution cannot be overemphasized. It enables the area of high stress to be identified at a glance. The computer program gives a wealth of information. However, it is a tedious procedure to extract the results from the data and caution must be applied in the interpretation of the results.

CONCLUSIONS

1. For separate horizontal and vertical loading, increasing B/D and A_f/A_w results in an increased level of transverse bending stress at the junction of hull and cross-structure.
2. For the combined loading, the decrease in transverse bending stress at the junction with increasing B/D and A_f/A_w is not considered applicable to a prototype structure due to the excessive horizontal load.
3. Away from the junction, increasing A_f/A_w and decreasing B/D results in a general reduction in transverse bending stress. Again, due to the excessive horizontal loading, applicability to a prototype structure is questionable for the combined loads.
4. Shear stress (τ_{xy}) at the junction generally increases with increasing A_f/A_w and increasing B/D.
5. Shear stress (τ_{xy}) at points other than the hull cross-structure junction generally increases with decreasing A_f/A_w and increasing B/D.
6. Maximum shear stress (τ_{max}) occurs along the top and bottom edges of the unstiffened models.
7. The vertical distribution of maximum shear stress (τ_{max}) is approximately constant for the stiffened models. The best correlation occurs with the higher values of A_f/A_w and lower values of B/D.

8. The vertical distribution of transverse bending stress due to vertical loading is very nearly linear, suggesting that the stress may be between that predicted by standard beam theory and deep beam theory.

9. A limiting value of A_f/A_w above which further reduction in the level of transverse bending stress would not occur was not determined. The data, however, suggests that such a limit does exist.

10. The results for those stresses calculated at the junction of hull and cross-structure are applicable only to other catamarans of similar junction configurations.

11. The results for those stresses calculated at points away from the junction should be applicable in a general sense to other cross-structures of similar design.

12. Used together, the photoelastic and computer methods of stress analysis should prove to be a valuable aid to the designer.

RECOMMENDATIONS

The information gained in this thesis is but a small part of that required to properly design the cross-structure of a large catamaran. Future investigations should concentrate on the determination of the effective breadth of deck plating that is resisting transverse bending. Additional information is required too, to substantiate the observation that most of the depth of the bulkhead web contributes to the bending resistance. It is doubtful that further work on a two-dimensional scale would be of any significant value. Therefore, it is recommended that any other experiments be done on a three-dimensional scale.

APPENDICES

APPENDIX A

SUPPLEMENTARY BACKGROUND INFORMATION

Photoelastic Analysis

The photoelastic technique of studying stress distribution within a model has become an everincreasing effective method of stress analysis since first being observed by Brewster in 1916. The basic technique itself is quite simple. A model is made of a birefringent material, placed in a loading frame and stressed. Using a polariscope, polarized light is directed through the model. In accordance with Snell's law, the light is refracted by the model, its velocity being changed in proportion to the index of refraction. The birefrigent property of the model material causes the light beam to be resolved along the two planes of principle stress. The velocity of transmission along each plane is dependent upon the stress intensity in the model. The light, traveling along the two principle planes, emerges from the model out-of-phase. The light then passes through the analyser, a polarizing device with its axis normal to that of the original polarizing unit. Upon passing through the analyser, the two transmitted light components either augment each other or cancel one another. This results in a series of dark or colored bands appearing on the viewing screen. These interference bands or lines are called isochromatics. Other lines called isoclinics can be used for finding the stress directions.

Isoclinic lines are obtained when a plane polariscope is used. The lines are defined as the locus of points at which the principle stress direction coincides with the direction of polarization. The lines appear as black lines across the model when either monochromatic or white light is used. The isoclinic pattern is obtained by rotating the polarizer and analyser simultaneously, usually in increments of about ten degrees, and tracing the resulting black lines. In order to obtain better definition of the isoclinics, a relatively insensitive birefrigent material should be used for the model. If isoclinics are desired, plexiglass is a suitable material. Isoclinics are necessary to construct principle stress patterns and are useful in making a quantitative analysis of the principle stresses.

Isochromatic lines appear as colored patterns if white light is used or as black lines if a monochromatic light source is used. The lines are known as fringe orders or orders of interference. They are defined as the locus of points of constant difference between principle stresses, $(\sigma_1 - \sigma_2)$. Additionally, since maximum shear stress is defined as $(\sigma_1 - \sigma_2)/2$, the lines also represent the locus of points of constant maximum shear stress. In order to best observe the isochramatic lines, a sensitive birefringent material should be used for the models.

When a stressed model is viewed through a plane polariscope, both the isoclinic and isochromatic lines will appear. In order to eliminate the isoclinic lines, quarter wave plates are placed between the model and the polarizer and analyser. These plates are made such that they cause a relative retardation of one quarter of the monochromatic wave length being used. The light now emerging from the analyser is in a condition which is termed circular polarization. The circularly polarized light is non-directional in nature, hence it is not effected by the directionality of the principle stress axes on the model.

It can be shown that:

$$(\sigma_1 - \sigma_2) = \frac{fn}{h}$$

where: f is the fringe constant of the model material (pounds per inch-order)

n is the order of interference

h is the thickness of the model (inches).

In order to determine the difference between the principle stresses at a point, it is only necessary to determine the order of interference at that point. The quantity $(\sigma_1 - \sigma_2)$ is then obtained using the above formula.

The order of interference is determined by first locating a point of zero order and then counting the lines to the point in question. The points of zero order are found by observing the growth of the fringe pattern while loading the model;

noting those lines or areas which remain dark through the entire loading process.

Since for this thesis it was only possible to obtain a value of $(\sigma_1 - \sigma_2)$ at various points, only the isochromatic fringe patterns were obtained. References (4), (6), and (8) should be consulted for a more detailed discussion of photoelastic theory, the polariscope and reduction of data from the fringe patterns.

Finite Element Analysis

The finite element method of stress analysis has been used in the aero industry for some time, and is now coming into more widespread use as a tool for analysing the stresses developed in a ship's hull. In the method, a real continuous structure is represented by a large number of small elements (plates, beams, etc.) whose elastic properties are taken to closely approximate those of the real structure. A set of simultaneous equations are generated by the application of the conditions of compatibility of deflections and equilibrium of forces at the joints or nodes of the connecting elements. The solution of this set of equations results in an approximation to the stress distribution in the real structure. It is most convenient to use matrix algebra to solve the equations thereby facilitating the use of a computer in setting up and solving the equations.

The computer program used for this thesis was provided by the Naval Ship Research and Development Center (NSRDC), Washington, D. C. The program was first written by J. R. Paulling of the University of California. It was later modified for use on the IBM 360/91, and enlarged to include other element types. This later work was done at NSRDC.

Paulling's work is described in Reference (12), while Reference (2) provides a good general overview to the method of analysis. For a detailed description of the method at a text book level, Reference (13) should be consulted.

Scaling

In the modeling of a real structure, there must exist a certain relationship between the linear dimensions of the model and the prototype. It has been shown using the theory of elasticity, and verified experimentally, that the difference in Poisson's ratio between metal and plastic has little effect on the magnitude or distribution of the stress. The significance of this being that it is not necessary to scale the thickness between model and prototype. This is important since the thickness of the photoelastic models used in this thesis is of the same order of magnitude as the thickness of the actual catamaran bulkhead.

The above ensures that the stress distribution results of the unstiffened models (#1, #5, #9) may be applied directly to the full scale prototype. If it is assumed that the strain

in the thickness direction caused by the stiffening of the remaining models is negligible, then these results may also be applied to the full scale prototype. Examination of the fringe order patterns would indicate that this is a valid assumption.

A constant length ratio between prototype and model was maintained for all models with respect to breadth and depth dimensions. It was not possible, however, to apply the same scale factor to the dimensions of the stiffening members. This was so because the scaling was not compatible in perpendicular directions.

In scaling the stiffening member, the cross-structure with its associated "effective breadth" of deck plating was taken to be a large plate girder, with the bulkhead acting as the web and outside deck plating acting as the two flanges. The ratio of total flange cross-sectional area to web cross-sectional area was determined. This ratio was then applied to the model in order to determine the "effective breadth" of plating for a given thickness of photoelastic plastic. From the above, the ratio A_f/A_w was defined and became one of the model parameters.

APPENDIX B

DETAILS OF PROCEDURE

General

The accomplishment of this thesis was facilitated a great deal by the work done in References (1), (10), and (11). These theses provided valuable details as to polariscope use, model preparation, experimental technique and data presentation.

After studying these references and other sources on the cross-structure problem, an experimental procedure was formulated to accomplish the thesis objectives. As a result of this formulation, the model parameters discussed previously were established and the following steps were carried out.

Model Preparation

The material selected to construct the models from was PSM-1, manufactured by Photolastic, Inc., of Malvern, Pennsylvania. The primary reasons for its selection were its high sensitivity and freedom from creep and edge effects. The latter makes this an excellent material for experiments that are to be conducted over a relatively long period of time. Further, it enables selective loadings to be rerun to check the photographic results. PSM-1 does offer some disadvantages, however. Its high sensitivity makes it vertually useless for determining isoclinics. A more serious drawback, for my purposes, was its very high sensitivity to heat when being cut. It appeared that even low

heat generation would cause residual stresses to be developed in the material. For this reason the cutting and machining of the models were very tedious and time consuming. In any further work, it is suggested that a less sensitive material such as PSM-5 be used if the models are not to be professionally made. The physical characteristics for all of photoelastics materials are contained in Reference (15).

In order to use the high speed cutter in the Ship Structures Laboratory for final cutting of the model it was necessary to make a metal template of the model outline. This was done by tracing the model outline from Reference (16) onto a sheet of 1/16" aluminum using the planograph in the Experimental Projects Laboratory. During the tracing, the scale was reduced by one half so that the model scale is 1/8" = 1'. While a thickness of 1/16" was used for the template, a 3/8" thickness would be more compatible with the high speed cutter. The metal template was then cut to the model outline and the edges smoothed. The band saw and sander in the student machine shop were used for these operations.

PSM-1 comes with a protective paper covering that can be drawn on to outline cuts, etc. The metal template was used to trace the model outline on the PSM-1 material. The models were then rough cut using the band saw in the Materials Processing Laboratory. The saw blade used should be as coarse as possible to reduce heat generation. The one used

for this operation had 14 teeth per inch. In addition, a jet of compressed air was directed on the model to cool it. With these procedures, the heat generated was kept to an acceptable level. When using PSM-1, the instructions contained in Reference (17) should be followed as closely as possible.

After being rough cut, the models were cut to their final dimensions using the high speed cutter in the Ship Structures Laboratory. The cutter turns at 45,000 RPM, consequently extreme care must be used for safety reasons and to prevent heat generation. Double stick tape was used to attach the models to the template.

In order to provide reference points for later comparison with the computer results, the models were scribed with the element outlines as can be seen in the fringe pattern photographs. Should any additional work be undertaken in this field, the inclusion of more elements would be helpful for comparison over a larger area of the model.

The various deck flange stiffeners were then cut from 1/8" sheets of PSM-1 in the same manner as above. The top stiffeners were glued to the models using a resin PC-1, and hardener PCH-1, supplied by Photolastic, Inc. The properties of this adhesive are listed at the end of this Appendix. The resin and hardener were mixed according to directions provided. An electric scale in the Civil

Engineering Laboratory was used to accurately determine the weight of each component.

With the top stiffeners in place, a series of fringe photographs were made to observe the effect of this stiffening. After completing these tests, the bottom stiffeners were added in the same manner as above.

Difficulty was encountered in applying the adhesive as it tends to run out of the joint. As can be seen in the fringe photographs, the adhesive tends to obscure the fringe orders. Masking tape was used in an attempt to prevent this, however, it did not work satisfactorily. In future work, perhaps tape with greater bonding would not allow quite so much leakage. In any case, the tape should be removed within an hour of adhesive application in order to prevent bonding of the tape by the adhesive.

Polariscope Description, Alignment and Use

The polariscope in the Ship Structures Laboratory was used for all photoelastic experiments. Pertinent name-plate data is provided at the end of this Appendix. The elements of the polariscope may be divided into two groups, one on either side of the model loading frame. On one side of the load frame is the short optical bench consisting of a steel track with light source housing, collimating lens and polarizer assembly. The other group is the long optical bench which includes the analyser assembly, a condensing or field lens, a camera lens, and the viewing screen or film

holder. Figure B-1 indicates the arrangement of the various elements.

The light source may be used to provide either white light or mercury green light. The two lamps are mounted on a turntable inside the light housing. A particular light may be brought into position by turning the knurled disk on the under side of the housing. Independent switches allow the selection of either light. When using the mercury light, the switch is placed in the ON position and the START button pushed on the outside power source. A masking plate with two holes of different diameters, 1.5 mm and 3.0 mm, is located on the front of the housing allowing some control over the amount of light emitted from the source.

The collimating lens is provided to convert the light emitted from the source into parallel light rays. This lens precedes the polarizer assembly which is composed of a polaroid disk mounted in a ring frame, and a quarter wave plate that can be swung into or out of the light path by means of a friction bolt. Both polarizer and quarter wave plate can be rotated within their frames independently. A pointer is attached to each of the rotating plates. An angular scale is scribed on each stationary frame which reads from 0° at the horizontal to 90° at the vertical. When the polarizer pointer is set at 90°, the axis of the polarizer is vertical.

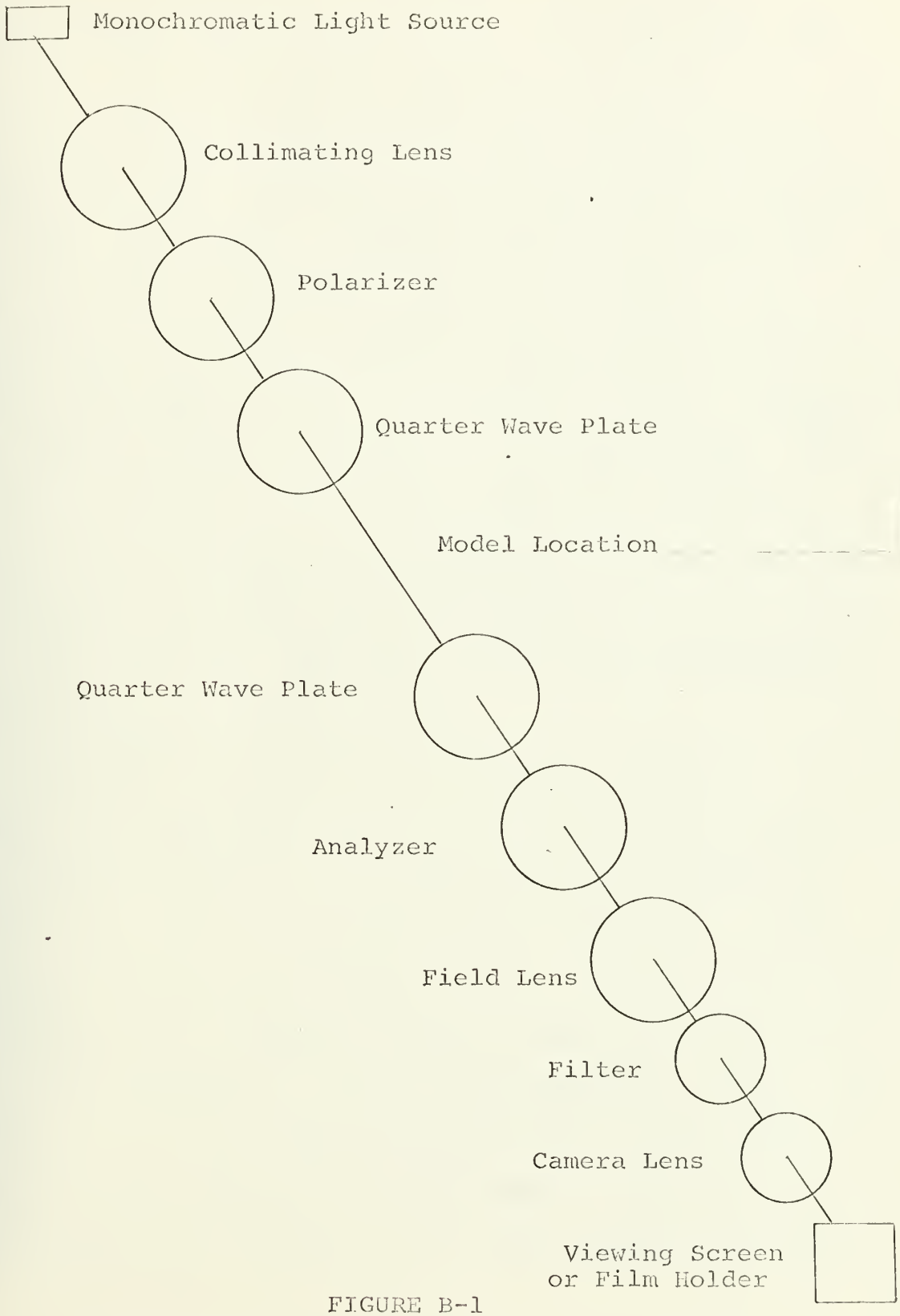

FIGURE B-1
SCHEMATIC OF STANDARD CIRCULAR POLARISCOPE

The analyser assembly is the first component on the long optical bench. It is identical to the polarizer assembly except that the quarter wave plate precedes the analyser. When the analyser pointer is set to 90°, its axis is horizontal. When all the plates are set to 90°, a standard circular polariscope with a dark field is obtained.

After the analyser assembly, the field or condensing lens causes the light rays to become convergent on the camera lens. Associated with the camera lens is a dark green filter which is used in conjunction with the mercury vapor lamp in making isochromatic fringe photographs. The filter is attached to the lens by means of a friction sleeve. It can be removed by holding the lens and twisting the filter. The camera lens is attached to the bench track on a rack and pinion arrangement which allows longitudinal adjustments to be made to the lens.

The camera shutter board is such that its hood engages the camera lens while allowing the viewing screen/ film holder section to move longitudnally to increase or decrease the size of the model image on the screen. The viewing end of the camera box contains a knob by which fine adjustments to the image size may be made. The camera box has several methods to view or record the model image. One method is to use the vertical ground glass screen which is attached to the camera by its own frame. Associated with this screen is a standard 8" x 10" film holder which slides

in front of the glass screen for picture taking. The screen is mounted in such a manner that when the model image is as desired, the film holder upon insertion, displaces the screen so that the film holder is at the same distance from the camera lens as the screen was, thereby preserving the size of the model image. In addition to the vertical screen, a horizontal tracing table is provided for tracing of the isoclinics. The table attaches in the same manner as the viewing screen and utilizes a mirror inclined at 45° to project the model image on the bottom of the tracing area. Because of the added distance the light must travel, the size of the image on the table is larger than that with the viewing screen. Consequently, the longitudinal position of the camera box must be adjusted to maintain the same image size.

The polariscope does not provide a film holder for Polaroid film. Therefore, it was necessary to borrow a viewing screen and Polaroid 4" x 5" film holder from the Experimental Stress Analysis Laboratory. The name plate data for both pieces of equipment is included in this Appendix. In order to use the 4" x 5" viewing screen with the polariscope, an adaptor frame is required. Such a frame had been made to accomplish the experimental work of Reference (1). This adaptor was used for this thesis. The 4" x 5" viewing screen must be removed from its backing plate and attached to the adaptor plate. The ground glass

screen is removed from its holder and the adaptor is inserted in its place. With this arrangement, it is then possible to use a 4" x 5" Polaroid film holder with the polariscope.

The aligning of the polariscope is a simple procedure, but it must be done to obtain accurate test results. The initial step is to position and level the two tables the optical benches are placed on, placing them on either side of and as close to the loading frame table as possible. Next, the two optical benches are placed on the tables with their ends as close to the loading frame as possible. The benches are then aligned and leveled. The alignment was accomplished by using a taut string. Shims, available in the Ship Structures Laboratory, were used for the leveling. Next, the light source was placed on and secured to the end of the short optical bench. The collimating lens was placed on the bench, its concave side towards the light source.

The correct position of the collimating lens is determined in the following manner. The white light source is turned on and a mirror is placed behind the lens, its plane perpendicular to the bench tracks. The lens is then moved longitudinally until the reflected image of the light source from the mirror back onto the face of the light source housing is the same diameter as the aperture in the masking plate. When the correct position is found, both the light source and lens are secured to the track by means of the locking screws.

Next, the polarizer assembly is placed on the track; the quarter wave plate being towards the loading frame. The whole assembly is placed as close as possible to the loading frame and secured to the track.

The next item is the loading frame, but since this is not an actual part of the polariscope it will be discussed separately in the next section.

The analyser assembly is now placed on the long optical bench with its quarter wave plate nearest the loading frame. Like the polarizer assembly, the analyser assembly is placed as close to the loading frame as possible and secured to the track. Next, the field lens is positioned approximately five inches from the analyser assembly. This distance is not critical, however, it does determine how much adjustment length will be available for the camera box.

After the field lens is secured in place, the camera lens is placed on the track. Its correct placement is determined by passing white light through the system and positioning the camera lens at that point where the field lens focuses the light to a point. It may also be necessary to adjust the long optical bench alignment so that the point of light is centered on the camera lens. If the light point is not centered, the model image will be distorted.

When the camera lens has been correctly positioned and secured, the hood of the shutter board is placed over the camera lens and secured to the track.

The polariscope should now be ready to use. Should the model appear to be slightly out of focus, this may be adjusted by means of the knob on the camera lens. Moving the viewing screen end of the camera box will have no effect on the image focus, only its size.

The film used for this experiment was Polaroid Type 52, a black and white 4" x 5" film. The advantage of using Polaroid film cannot be overemphasized. It allows an almost immediate check as to picture quality; a tremendous time saver to the some time photographer. The shutter board of the polariscope provides for shutter speeds of 1/2 to 1/50 sec as well as bulb and time positions. There is also an aperture adjustment from fully open to fully closed. The settings used for all pictures were .25 seconds, fully opened aperture, and the 3 mm opening in the masking plate. Polaroid does produce a film that gives a negative which would be useful in enlarging the model image to determine fringe orders. Reference (1) provides guidance in this area.

Loading Frame and Model Loading

The loading frame used in this experimental work is located in the Ship Structures Laboratory. It was originally designed and built for the work done in Reference (18). Over the years it has been modified for other thesis work, however, it still remains a good loading frame. Since the models tested in this thesis required only simple supports, further modification of the frame was not necessary. The

device consists primarily of a platform and load support members. The platform can be adjusted to aid in the positioning of the model on the viewing screen. The entire loading frame was mounted on a vertically adjustable steel table borrowed from the Experimental Stress Laboratory. This feature and the transversely adjustable loading frame were an invaluable aid since the model position in the polariscope could be adjusted without disturbing the model or its loading.

The models were supported on small steel blocks with curved bearing surfaces. Knife edges are not suitable in this work since they tend to damage the plastic and cause residual stresses where the plastic deforms. The load was applied to the model using a hydraulic ram and a 3/4" x 1/8" diameter steel pin. A small piece of lead sheet was placed between the pin and model to prevent damage to the model. Name plate data for the ram and pump are provided at the end of this Appendix. A 0-200 psi gage was used to determine the pressure on the ram. The gage was calibrated using the dead weight tester in the Experimental Projects Laboratory. The gage reading was multiplied by the ram area to obtain the load on the model.

While this method of supporting and loading the model was satisfactory, it is felt that a restraint to prevent any out-of-plane bending of the model would improve the accuracy of the results.

Test Procedure

With the models prepared and the polariscope alignment completed as previously described, actual testing could be undertaken.

The mercury light was started, the green filter installed over the camera lens, and the horizontal tracing table was installed on the end of the viewing screen. The tracing table was used because the physical limitations of the hydraulic pump and ram prevented simultaneously loading and viewing of the model if the vertical viewing screen was used.

The model was then placed in the loading frame and positioned so as to provide symmetrical loading with respect to the model centerline. In addition, the model was checked to ensure that its vertical plane was perpendicular to the light beam. With the model in satisfactory position, a small load was applied to the model to make sure the loading was symmetrical.

With these steps complete, the model was loaded slowly to observe the location of the zero fringe order and the general pattern of fringe order formation. This knowledge is vital in order to correctly interpret the fringe order photographs.

The load on the model was then reduced to zero to prevent any overstraining. The tracing table was removed and the vertical 4" x 5" viewing screen installed. The size of the model image was adjusted so as to make it as large as possible, yet retain as much as possible of the model outline.

With the model in the correct position, the film holder and film were inserted, the model reloaded, and the picture taken.

Again, to prevent any overstraining, the model was unloaded. Next the picture was processed and checked for clearness, contrast, proper exposure, etc. If the picture was satisfactory, the model was removed from the loading frame and another one set up. In all, forty-two loadings were performed and photographed. The results of those tests, both numeric and photographic, are contained in Appendices C and D respectively.

Computer Procedure

During the same time period that the photoelastic models were being made, a finite element computer model was established. An element grid was made over the actual model size as shown in Figure E-1. These elements were then transformed into computer input data in accordance with Reference (14). A sample of input data is provided in Appendix D.

After the model tests were completed, runs were made on the computer with loading identical to that on the photoelastic models. In addition, the computer was programmed to give results of combined vertical and horizontal loading. This loading was not included in the photoelastic model results. Due to monetary limitations, computer runs were not made for those tests in which the model was stiffened on the top only.

The computer output is quite comprehensive, providing stress and stress gradients for the x and y directions and the shear stress for each element entered as input. It was not considered necessary that all of this information be included with this thesis. That information that was required for comparison with the photoelastic models, and thought to be of special interest was extracted from the output and is included in Appendix C.

Model Configuration

The following table presents the configuration of each of the models tested along with the corresponding parameter of the full scale prototype.

TABLE B-1

MODEL-SHIP PARAMETERS

MODEL	D_m	B/D	FW_m	A_f/A_w	FW_s	D_s
1	2.6875	4.0	0	0	0	21.5
2	2.6875	4.0	1.50	.558	4.0	21.5
3	2.6875	4.0	1.12	.419	3.0	21.5
4	2.6875	4.0	.750	.279	2.0	21.5
5	2.175	5.0	0	0	0	17.4
6	2.175	5.0	1.50	.690	4	17.4
7	2.175	5.0	1.12	.517	3	17.4
8	2.175	5.0	.750	.345	2	17.4
9	1.8125	6.0	0	0	0	14.5
10	1.8125	6.0	1.50	.828	4	14.5
11	1.8125	6.0	1.12	.620	3	14.5
12	1.8125	6.0	.750	.414	2	14.5

D_m: Depth of model cross-structure (inches)

B/D: Breadth to depth ratio for model and ship

FW_m: Calculated deck flange width, model (inches)

A_f/A_w: Ratio of total (upper and lower) deck flange cross-sectional area to web cross-sectional area

FW_s: Assumed deck flange width, ship (feet)

D_s: Depth of ship cross-structure (feet)

Determination of Material Fringe Constant

Although the manufacturer provides the fringe constant for the particular material being used for model construction, it is possible that it can vary. For this reason, and the fact that the photoelastic plastic for this thesis had to be specially cast, a determination of the fringe constant was considered necessary.

There are three primary methods of calculating the fringe constant; tensile test, simple bending, and compression of a circular disk. Since all of the models would be tested under a bending load, the simple bending method of determining the fringe constant was considered most appropriate.

The test procedure and calculations are relatively simple and straightforward. A test beam with dimensions as shown in Figure B-2 was manufactured in the same manner as the models. A load was applied to the beam so as to produce approximately five fringe orders on either side of the neutral axis. A photograph of the stress pattern was made

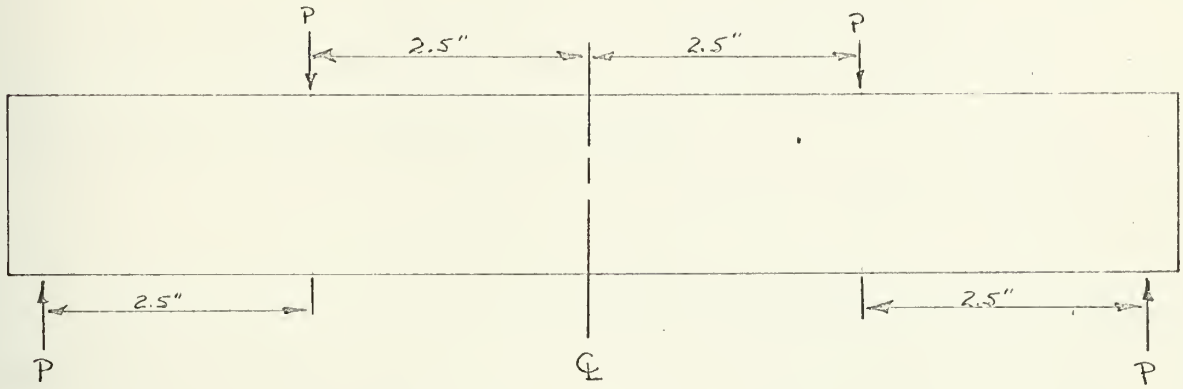

(a) CALIBRATION BEAM

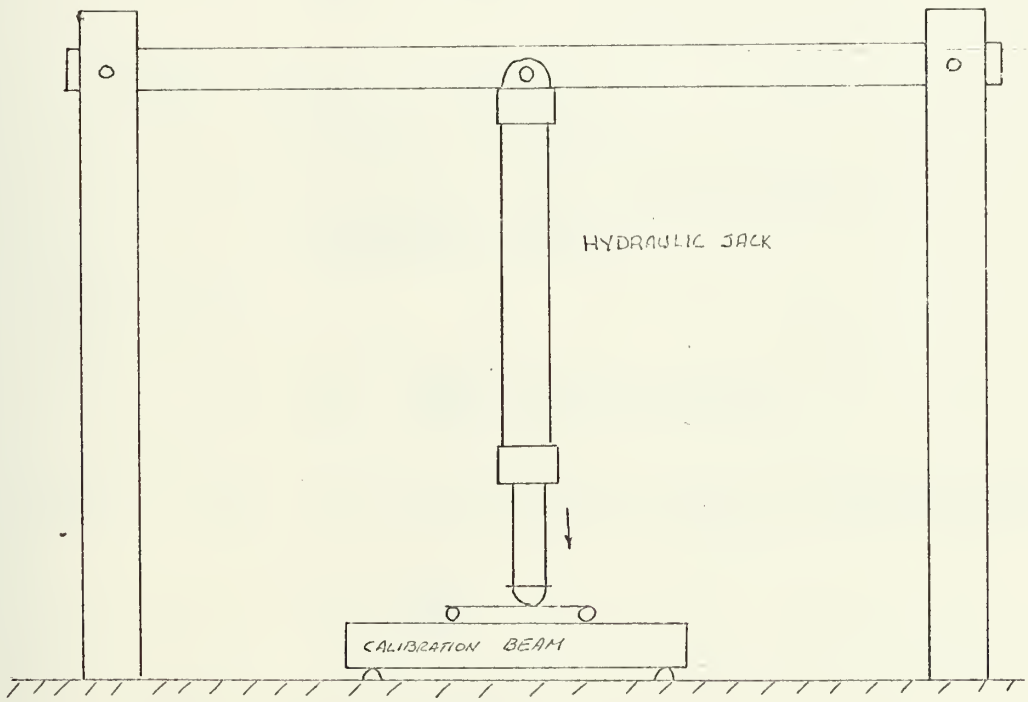

(b) LOAD FRAME FOR CALIBRATION

FIGURE B-2
CALIBRATION BEAM AND LOADING

and the amount of load recorded. Using these photographs, the fringe order was determined as illustrated in Figure B-3.

When a beam is loaded in simple bending, the principle stresses are along and normal to its free boundaries. Since the normal stress must be zero at a free boundary, the photoelastic stress equation becomes

$$\sigma = \frac{fn}{h}$$

Combining this equation with the bending stress equation for a beam results in

$$\frac{Mc}{I} = \frac{fn}{h}$$

where M: Bending Moment

I: Moment of Inertia

c: Distance from neutral axis to outermost fiber

Rearranging

$$f = \frac{Mch}{In} \text{ (lb/inch-order)}$$

For this test the bending stress can be expressed as

$$\sigma = \frac{Pa6}{hb^2}$$

where P: Load (lbs)

a: Moment Arm (in.)

b: Height of Beam (in.)

substituting gives

$$f = \frac{Pa6}{nb^2} \quad \text{(lbs/inch-order)}$$

Table B-2 gives the results of the fringe constant calculations.

TABLE B-2

CALCULATION OF FRINGE CONSTANT

	Run 1	Run 2	Run 3
Total load (lbs)	99.4	99.4	99.4
P(lbs)	49.7	49.7	49.7
a(in)	2.5	2.5	2.5
n	4.40	4.65	4.406
D(in) (ave meas val)	2.018	2.018	2.018
f(lbs/inch-order)	41.60	39.36	41.54
f (average)	40.8		

TABLE B-3

PROPERTIES OF PSM-1 PHOTOELASTIC MATERIAL

E	340,000 psi
f	40 lb/in-order
ν	.38
Lot #	0041
Thickness	1/4 inch
Mfr.	Photolastic, Inc. Malvern, Pennsylvania

TABLE B-3(Cont'd)

PROPERTIES OF ADHESIVE

Resin Type	PC-1
Hardner Type	PCH-1
Cure Time	12 hrs.
Cure Temperature	Room
Elongation	3-5%
E	450,000 psi
Mfr.	Photolastic, Inc. Malvern, Pennsylvania

Apparatus Data

Polariscope:	Mfr: Polarizing Instrument Company Mt. Kisco, New York
	Lamps: Monochromatic - Westinghouse SAH-250A Mercury
	White - Westinghouse 500W 120V Projection
	Filter: Wratten #77
High Speed Cutter:	Chapman Photoelastic Model Maker
	Mfr: Chapman Laboratories West Chester, Pennsylvania
	HP: 1/4
	RPM: 45,000
Load Device:	Blackhawk Type P450 Hydraulic Pump
	with Blackhawk Type RC 540 Ram.
	Ram Area: .994 sq. in.
Film Holder:	Polaroid Type 500 4" x 5" Film Holder
Film Type:	Polaroid Type 52 4" x 5" Film
Viewing Screen:	Component of Nikon transmission
	polariscope, located in Experimental
	Stress Analysis Laboratory.

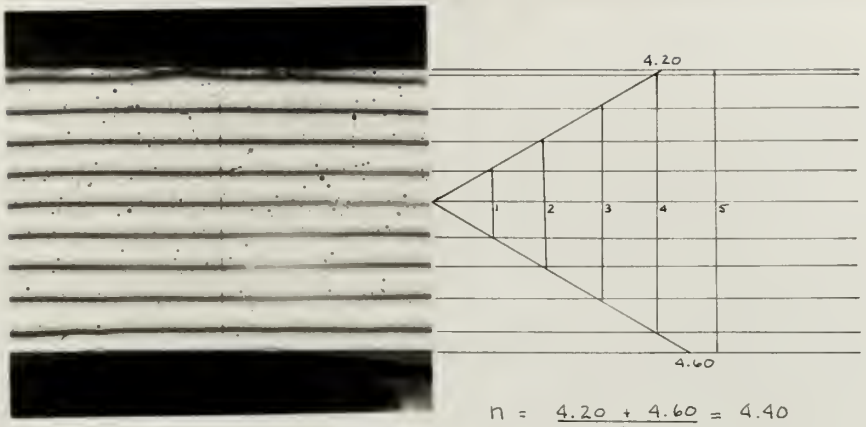

RUN # 1

$$n = \frac{4.20 + 4.60}{2} = 4.40$$

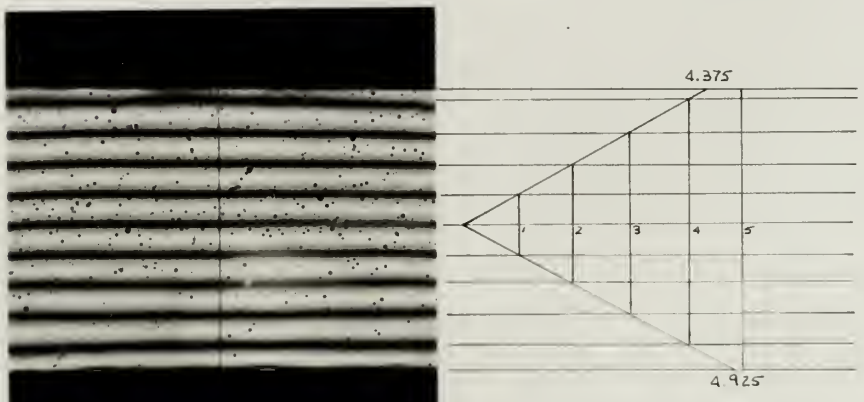

RUN # 2

$$n = \frac{4.375 + 4.925}{2} = 4.650$$

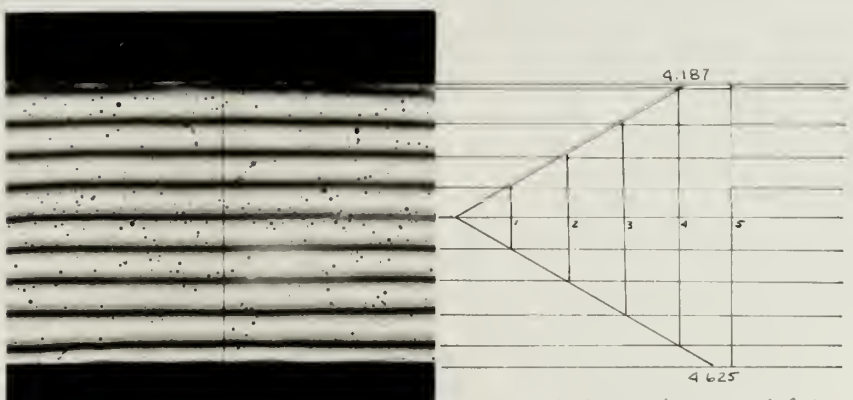

RUN # 3

$$n = \frac{4.187 + 4.625}{2} = 4.406$$

FIGURE B-3, CALIBRATION FRINGE ORDER

APPENDIX C

SUMMARY OF DATA

Interpretation of Computer Output

As numerically competent as a computer is, it cannot reason between output that seems correct and that which is in error. That is to say, the programmer or user is required to ascertain the significance of all the data presented to him.

Depending on the wishes of the user, the FINEL program will provide node displacements, forces acting at the nodes and member stresses. The output selected for this thesis was a combination of node displacements and member stresses.

The member stress output is dependent on the type of member element selected. For a bar, axial stress only is provided. For rectangular and quadrilateral elements, stresses, stress gradients, and shear stress are provided. If a triangle is used, output consists of stresses, shear stress, and principle stresses and their directions. Figure C-1 illustrates the two-dimensional elements used for this thesis.

If the element stress results for a particular problem are plotted, it will be found that, in general, the stresses for adjacent elements do not match along their boundaries. This is inherent in any finite element solution. The amount of mismatch may be improved by reducing the size of the elements, but it cannot be eliminated. The problem then arises of choosing those stresses which more closely approximate the actual stresses.

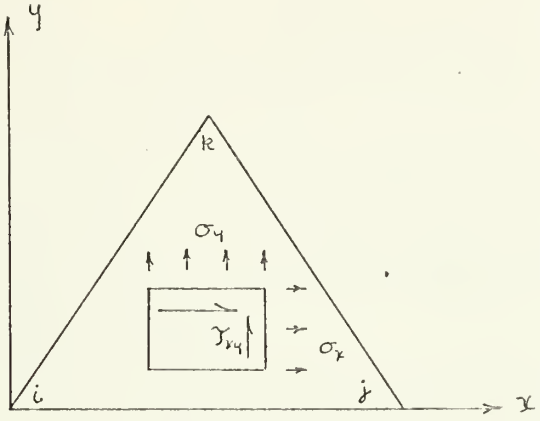

Triangle

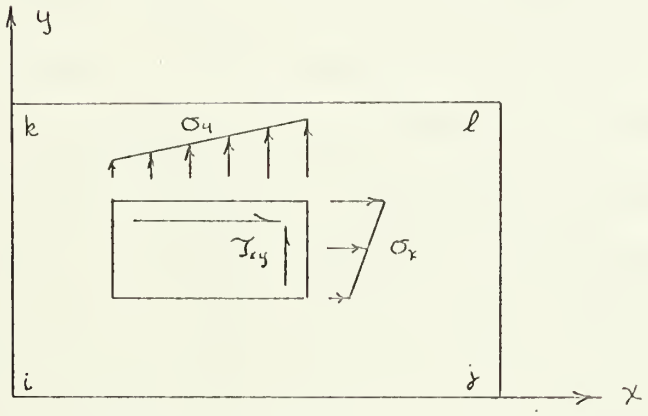

Rectangle

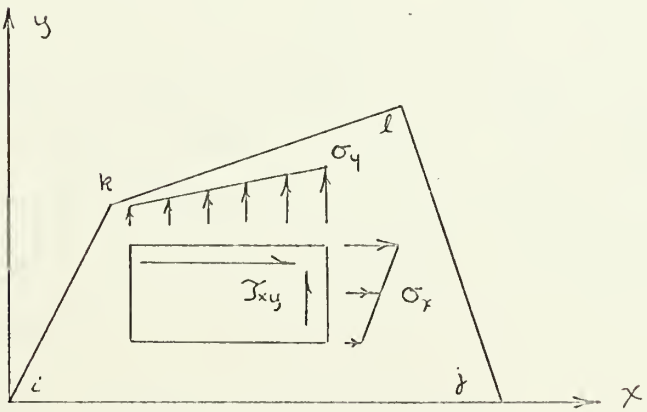

Quadrilateral

FIGURE C-1
TWO-DIMENSIONAL PLATE ELEMENTS

Zienkiewicz, in Reference (13), provides some guidance in interpreting the results. For a condition of plane stress or strain, the overall stress level as calculated by finite element methods will be lower than that calculated by an exact theory. The accuracy of the results will depend on the type of stress field, type of element being used, and the fineness of the element grid.

If a triangle is used in a uniform stress field, then the exact solution will be given. However, if the triangle is used in a linearly varying stress field, the results will not be as accurate since the triangle provides only a constant stress output as is indicated in Figure C-1. For this case, more accurate results are obtained if the stresses around a node are averaged. Zienkiewicz further cautions that when using triangular elements, the stresses calculated at internal nodes are more accurate than those at outside edges. Use of rectangular or quadrilateral elements is preferred because the stress results are given as corner point stresses plus a stress gradient, thereby enabling the stress variation over the element edge to be calculated. No matter which element is used, accuracy may be improved by reducing the overall mesh or element grid size, with further reduction around suspected areas of stress concentrations.

Utilizing the above guidelines, the results of the FINEL program were interpreted and stresses chosen which were thought to give the best representation of the actual

stress distribution. The stress values selected were chosen in the following manner:

(a) VERTICAL DISTRIBUTION OF TRANSVERSE BENDING STRESS
(TABLES C-1, C-4, C-7)

The corner point stress of each element along a particular node line was chosen. The stress at the bottom of the cross-structure was calculated from the element corner point stress plus the stress gradient in the vertical direction. The bar stresses were not chosen because of the necessity to compare stresses with the unstiffened models and the photoelastic models. Also, the bar stresses are not as accurate as those in the rectangular elements.

(b) VERTICAL DISTRIBUTION OF SHEAR STRESS
(TABLES C-2, C-5, C-8)

The element shear stress along a particular node line was chosen. It is assumed to act at the midpoint of the element side.

(c) TRANSVERSE BENDING AT THE BOTTOM OF THE CROSS-STRUCTURE
(TABLES C-3, C-6, C-9)

Stress was calculated in the same manner as for the bottom stresses in (a) above.

(d) TRANSVERSE STRESS AT JUNCTION OF CROSS-STRUCTURE AND HULL

This stress was determined in the same manner for both (a) and (b) above. It was calculated using the corner point stress of element 77, plus its stress gradient in the vertical direction. This stress was used vice that of

element 87, since it is assumed that the stress in a triangular element acts at its midpoint. This assumption then places the stress of element 87 outboard of the line of node 8 (see Figure D-1).

TABLE C-1

TRANSVERSE BENDING STRESS

MODEL VERTICALLY LOADED

LOAD: 99.4 lbs.

ROW	ELEM	σ	ELEM	σ	ELEM	σ	ELEM	σ
MODEL #1								
1	17	-835.89	15	-705.9	13	-594.53	11	-508.60
3	37	-803.20	35	-496.62	33	-412.11	31	-343.95
3	57	-266.82	55	-336.7	53	-243.46	51	-229.01
4	69	308.48	68	244.17	67	166.22	66	147.94
5	79T	714.79	78T	535.01	77T	474.69	76	343.47
6	79B	1076.79	78B	1134.01	77B	427.49	86	402.26
MODEL #2								
1	18	-339.89	16	-279.90	14	-241.10	12	-210.65
2	37	-435.77	35	-217.26	33	-186.79	31	-152.78
3	57	-85.26	55	-166.96	53	-127.00	51	-106.64
4	69	146.65	68	110.43	67	84.98	66	73.66
5	79T	286.95	78T	268.45	77T	208.32	76	213.62
6	79B	362.25	78B	332.85	77B	576.82	86	413.18
MODEL #3								
1	18	-399.27	16	-327.42	14	-281.26	12	-244.88
2	37	-474.12	35	-248.55	33	-212.82	31	-175.23
3	57	-105.84	55	-186.00	53	-143.10	51	-121.22
4	69	162.01	68	122.68	67	92.45	66	80.02
5	79T	328.97	78T	295.38	77T	232.58	76	225.71
6	79B	437.69	78B	401.18	77B	564.58	86	413.02

TABLE C-1
(Cont'd)

MODEL #4

ROW	ELEM	σ	ELEM	σ	ELEM	σ	ELEM	σ
1	18	-484.50	16	-395.15	14	-338.27	12	-293.08
2	37	-529.85	35	-293.24	33	-249.61	31	-206.73
3	57	-135.02	55	-213.02	53	-165.66	51	-141.55
4	69	185.43	68	141.52	67	104.01	66	90.03
5	79T	391.78	78T	335.47	77T	269.46	76	243.49
6	79B	548.98	78B	505.15	77B	545.46	86	412.14

MODEL #5

1	37	-1286.60	35	-1137.82	33	-967.22	31	-806.38
2	57	-1153.19	55	-837.97	53	-677.51	51	-575.02
3	69	246.59	68	116.36	67	88.33	66	79.50
4	79T	1005.84	78T	717.99	77T	611.38	76	434.90
5	79B	1648.84	78B	1691.99	77B	627.88	86	543.90

MODEL #6

1	38	-466.24	36	-392.93	34	-342.04	32	-298.23
2	57	-491.41	55	-315.23	53	-261.00	51	-215.08
3	69	114.79	68	25.97	67	52.88	66	43.47
4	79T	365.26	78T	322.54	77T	231.72	76	253.47
5	79B	495.06	78B	452.10	77B	766.62	86	535.29

MODEL #7

1	38	-555.96	36	-466.75	34	-404.88	32	-351.31
2	57	-554.57	55	-367.82	53	-304.52	51	-253.18
3	69	124.93	68	32.19	67	54.20	66	44.23
4	79T	422.02	78T	358.34	77T	262.83	76	268.42

TABLE C-1

(Cont'd)

ROW	ELEM	σ	ELEM	σ	ELEM	σ	ELEM	σ
MODEL #7 (Cont'd)								
5	79B	604.62	78B	550.06	77B	757.83	86	539.34
MODEL #8								
1	38	-688.82	36	-575.50	34	-497.00	32	-428.11
2	57	-648.74	55	-445.23	53	-367.80	51	-308.21
3	69	141.52	68	42.84	67	57.27	66	46.64
4	79T	509.10	78T	413.14	77T	311.45	76	291.66
5	79B	770.86	78B	703.70	77B	742.65	86	544.55
MODEL #9								
1	57	-2119.48	55	-1732.60	53	-1391.59	51	-1153.12
2	69	-182.74	68	-71.96	67	-101.34	66	-76.19
3	79	1330.49	78	835.35	77	755.11	76	506.40
4	79	2324.49	78	2366.35	77	854.81	76	727.40
MODEL #10								
1	58	-622.12	56	-524.36	54	-450.24	52	-385.57
2	69	-153.83	68	-30.79	67	-5.69	66	.78
3	79T	466.09	78T	316.05	77T	261.52	76	284.37
4	79B	630.77	78B	577.05	77B	950.02	86	658.11
MODEL #11								
1	58	-752.50	56	-631.18	54	-538.29	52	-458.47
2	69	-159.17	68	-38.33	67	-16.96	66	-9.99
3	79T	535.13	78T	358.14	77T	297.23	76	300.08
4	79B	775.77	78B	706.98	77B	946.59	86	666.73

TABLE C-1

(Cont'd)

MODEL #12

ROW	ELEM	σ	ELEM	σ	ELEM	σ	ELEM	σ
1	58	-953.17	56	-794.08	54	-670.49	52	-566.64
2	69	-165.66	68	-47.94	67	-32.59	66	-24.51
3	79T	643.95	78T	424.59	77T	354.99	76	325.68
4	79B	1002.83	78B	915.43	77B	939.27	86	679.63

σ: psi

T: Top of Element

B: Bottom of Element

TABLE C-2

SHEAR STRESS

MODEL VERTICALLY LOADED

LOAD: 99.4 lbs.

MODEL #1

ROW	ELEM	τ	ELEM	τ	ELEM	τ	ELEM	τ
1	17	38.02	15	74.79	13	70.14	11	69.74
2	37	308.79	35	181.01	33	173.10	31	163.92
3	57	205.20	55	242.04	53	235.86	51	228.40
4	69	90.52	68	162.23	67	208.79	66	191.51
5	79	28.52	78	-11.16	77	42.93	76	72.41

MODEL #2

1	17	130.63	15	108.48	13	100.08	11	99.12
2	37	270.72	35	152.93	33	145.15	31	139.87
3	57	162.30	55	185.52	53	180.99	51	178.01
4	69	99.48	68	145.62	67	189.05	66	202.19
5	79	84.82	78	110.76	77	226.24	76	155.03

MODEL #3

1	17	127.20	15	105.40	13	97.10	11	96.05
2	37	274.23	35	156.09	33	148.12	31	142.30
3	57	166.60	55	191.21	53	186.54	51	183.01
4	69	98.84	68	147.06	67	190.64	66	201.47
5	79	77.34	78	97.42	77	210.11	76	147.51

MODEL #4

1	17	121.84	15	1-0.70	13	92.67	11	91.57
2	37	279.60	35	160.73	33	152.51	31	145.92

TABLE C-2

(Cont'd)

MODEL #4 (Cont'd)

ROW	ELEM	τ	ELEM	τ	ELEM	τ	ELEM	τ
3	57	173.04	55	199.69	53	194.77	51	190.42
4	69	97.82	68	149.30	67	193.01	66	200.12
5	79	66.73	78	77.92	77	185.09	76	135.90
MODEL #5								
1	37	45.09	35	75.63	33	84.40	31	85.55
2	57	302.20	55	265.58	53	272.30	51	266.93
3	69	175.37	63	263.63	67	296.60	66	271.21
4	79	54.48	78	-.93	77	67.95	76	103.03
MODEL #6								
1	37	119.38	35	124.44	33	128.03	31	135.60
2	57	244.92	55	200.43	53	206.29	51	205.26
3	69	167.39	68	214.87	67	243.58	66	261.36
4	79	126.89	78	163.07	77	308.76	76	203.91
MODEL #7								
1	37	114.72	35	120.99	33	124.75	31	131.64
2	57	250.29	55	206.96	53	212.71	51	211.00
3	69	168.19	68	218.88	67	248.16	66	262.96
4	79	117.94	78	146.41	77	290.08	76	195.93
MODEL #8								
1	37	106.82	35	115.18	33	119.32	31	125.28
2	57	258.41	55	216.70	53	222.25	51	219.57

TABLE C-2

(Cont'd)

MODEL #8 (Cont'd)

ROW	ELEM	τ	ELEM	τ	ELEM	τ	ELEM	τ
3	69	169.43	68	225.17	67	255.01	66	264.89
4	79	104.48	78	121.68	77	259.97	76	183.11

MODEL #9

1	57	226.59	55	250.04	53	265.81	51	263.39
2	69	314.59	68	331.72	67	400.85	66	365.78
3	79	91.41	78	17.26	77	88.19	76	145.10

MODEL #10

1	57	203.79	55	206.28	53	222.89	51	230.55
2	69	286.83	68	245.55	67	296.51	66	317.75
3	79	177.39	78	223.39	77	381.10	76	251.67

MODEL #11

1	57	206.81	55	211.16	53	227.51	51	233.98
2	69	289.36	68	252.29	67	304.77	66	322.54
3	79	167.41	78	204.00	77	360.86	76	244.15

MODEL #12

1	57	211.04	55	218.17	53	234.16	51	238.87
2	69	293.31	68	263.01	67	317.57	66	329.42
3	79	152.75	78	174.60	77	327.36	76	231.65

TABLE C-3

TRANSVERSE BENDING STRESS AT BOTTOM OF CROSS-STRUCTURE

MODEL VERTICALLY LOADED

LOAD: 99.4 lbs.

MODEL	NODE (ELEMENT)					
	6(85)	7(86)	8(77)	9(78)	10(79)	11(80)
1	259.09	402.26	427.29	1134.01	1076.79	1128.19
2	230.25	413.18	576.82	332.85	362.25	396.41
3	233.52	413.02	564.58	401.18	437.69	475.69
4	238.14	412.14	545.46	505.15	598.98	591.36
5	353.12	566.76	627.88	1691.99	1648.84	1754.49
6	291.96	535.29	766.62	452.10	495.06	546.10
7	297.84	539.34	757.83	550.06	604.62	664.61
8	306.45	544.55	742.65	703.70	770.86	838.02
9	450.49	753.54	854.71	2365.35	2324.49	2523.56
10	350.88	658.11	950.02	577.05	630.77	703.16
11	358.91	666.73	946.59	706.98	775.77	861.10
12	371.49	679.63	939.27	915.43	1002.83	1105.17

TABLE C-4

TRANSVERSE BENDING STRESS

MODEL HORIZONTALLY LOADED

LOAD: 99.4 lbs.

MODEL #1

ROW	ELEM	σ	ELEM	σ	ELEM	σ	ELEM	σ
1	17	644.11	15	595.00	13	539.75	11	489.88
2	37	319.79	35	298.84	33	275.41	31	249.58
3	57	114.66	55	113.96	53	101.18	51	98.69
4	69	-374.03	68	-343.53	67	-209.29	66	-267.36
5	79T	-743.79	78T	-606.32	77T	-593.88	76T	-481.98
6	79B	-965.79	78B	-1360.32	77B	-669.88	76B	-581.48

MODEL #2

1	18	215.58	16	205.15	14	192.34	12	179.12
2	37	84.01	35	82.27	33	77.82	31	72.16
3	57	-.77	55	-.86	53	1.94	51	-.45
4	69	-204.67	68	-194.16	67	-191.07	66	-169.46
5	79T	-341.43	78T	-339.48	77T	-209.85	76	-322.96
6	79B	-364.15	78B	-454.80	77B	-760.09	86	-556.81

MODEL #3

1	18	258.30	16	244.74	14	228.40	12	211.90
2	37	107.65	35	104.26	33	98.14	31	90.77
3	57	10.93	55	12.29	53	12.31	51	9.86
4	69	-222.51	68	-209.23	67	-201.30	66	-178.96
5	79T	-382.56	78T	-367.42	77T	-318.75	76	-337.43
6	79B	-434.36	78B	-531.32	77B	-743.19	86	-560.79

TABLE C-4

(Cont'd)

ROW	ELEM	σ	ELEM	σ	ELEM	σ	ELEM	σ
MODEL #4								
1	18	321.99	16	303.31	14	281.30	12	259.62
2	37	142.79	35	136.76	33	128.01	31	117.93
3	57	28.28	55	29.21	53	27.52	51	24.96
4	69	-248.56	68	-231.41	67	-216.31	66	-193.09
5	79T	-442.87	78T	-408.41	77T	-360.70	76	-359.27
6	79B	-535.11	78B	-698.53	77B	-736.14	86	-567.44
MODEL #5								
1	37	920.27	35	843.01	33	755.77	31	666.67
2	57	530.14	55	493.64	53	438.46	51	399.98
3	69	-326.96	68	-296.41	67	-236.96	66	-215.64
4	79T	-909.32	78T	-723.90	77T	-700.64	76	-552.8
5	79B	-1301.92	78B	-1752.30	77B	-831.76	86	-751.96
MODEL #6								
1	38	266.34	36	255.17	34	238.93	32	220.84
2	57	128.59	55	121.47	53	113.65	51	102.52
3	69	-183.16	68	-174.32	67	-174.33	66	-151.99
4	79T	-378.64	78T	-376.44	77T	-318.55	76	-355.88
5	79B	-436.32	78B	-532.28	77B	-889.75	86	-646.10
MODEL #7								
1	38	324.23	36	308.71	34	287.25	32	264.05
2	57	164.26	55	155.16	53	144.12	51	130.94
3	69	-197.60	68	-185.76	67	-180.41	66	-157.39

TABLE C-4

(Cont'd)

MODEL #7 (Cont'd)

ROW	ELEM	σ	ELEM	σ	ELEM	σ	ELEM	σ
4	79T	-428.25	78T	-409.82	77T	-351.02	76	-372.53
5	79B	-525.69	78B	-629.54	77B	-884.46	86	-654.51

MODEL #8

1	38	413.27	36	390.22	34	360.02	32	328.37
2	57	219.02	55	206.48	53	190.02	51	173.42
3	69	-218.94	68	-202.89	67	-189.46	66	-165.69
4	79T	-502.73	78T	-459.86	77T	-400.87	76	-398.11
5	79B	-685.25	78B	-779.46	77B	-876.59	86	-667.75

MODEL #9

1	57	1217.84	55	1119.14	53	972.60	51	857.31
2	69	-187.72	68	-170.04	67	-110.85	66	-101.47
3	79T	-1061.53	78T	-823.41	77T	-789.90	76	-602.41
4	79B	-1682.65	79B	-2186.69	77B	-1004.90	67	-892.18

MODEL #10

1	58	315.70	56	305.98	54	286.67	52	259.94
2	69	-137.29	68	-132.91	67	-137.53	66	-116.12
3	79T	-403.81	78T	-401.89	77T	-335.43	76	-378.14
4	79B	-505.97	78B	-609.53	77B	-1013.87	86	-729.03

MODEL #11

1	58	388.70	56	373.93	54	347.30	52	313.24
2	69	-143.53	68	-136.39	67	-135.77	66	-114.02
3	79T	-459.97	78T	-438.96	77T	-370.76	76	-395.45
4	79B	-614.13	78B	-725.36	77B	-1013.44	86	-741.60

TABLE C-4

(Cont'd)

MODEL #12

ROW	ELEM	σ	ELEM	σ	ELEM	σ	ELEM	σ
1	58	504.09	56	480.15	54	440.53	52	394.44
2	69	-152.29	68	-141.44	67	-132.84	66	-111.07
3	79T	-546.28	78T	-495.85	77T	-426.29	76	-422.76
4	79B	-781.36	78B	-909.29	77B	-1013.09	86	-761.70

σ: psi

T: Top of Element

B: Bottom of Element

TABLE C-5

SHEAR STRESS

MODEL HORIZONTALLY LOADED

LOAD: 99.4 lbs.

ROW	ELEM	τ	ELEM	τ	ELEM	τ	ELEM	τ
MODEL #1								
1	17	-15.56	15	-27.31	13	-35.41	11	-40.62
2	37	-29.53	35	-54.90	33	-76.04	31	-85.98
3	57	-13.60	55	-46.09	53	-78.49	51	-100.03
4	69	46.74	68	29.19	67	-34.11	66	-49.72
5	79	19.77	78	153.49	77	121.45	76	70.23
MODEL #2								
1	17	-13.03	15	-26.14	13	-37.98	11	-46.68
2	37	-12.24	35	-29.68	33	-46.88	31	-59.82
3	57	2.32	55	-18.48	53	-47.43	51	-67.34
4	69	24.76	68	24.26	67	-49.78	66	-96.76
5	79	-7.67	78	73.15	77	-152.70	76	-50.36
MODEL #3								
1	17	-14.07	15	-27.29	13	-38.74	11	-46.94
2	37	-14.59	35	-32.92	33	-50.37	31	-62.90
3	57	.136	55	-21.70	53	-50.76	51	-70.54
4	69	26.70	68	24.99	67	-47.43	66	-91.81
5	79	-1.66	78	83.98	77	-126.64	76	-38.49
MODEL #4								
1	17	-15.23	15	-28.49	13	-39.35	11	-46.87
2	37	-17.86	35	-37.44	33	-55.29	31	-67.27

TABLE C-5

(Cont'd)

MODEL #4 (Cont'd)

ROW	ELEM	τ	ELEM	τ	ELEM	τ	ELEM	τ
3	57	-29.40	55	-26.36	53	-55.63	51	-75.32
4	69	29.57	68	25.90	67	-44.21	66	-84.59
5	79	6.08	78	98.90	77	-87.64	76	-20.92
MODEL #5								
1	37	-14.24	35	-30.22	33	-42.39	31	-46.77
2	57	-24.11	55	-67.91	53	-108.30	51	-132.80
3	69	40.04	68	4.51	67	-81.38	66	-100.29
4	79	16.96	78	174.31	77	121.94	76	56.28
MODEL #6								
1	37	-9.75	35	-28.87	33	-47.83	31	-61.99
2	57	-.72	55	-27.73	53	-63.31	51	-87.18
3	69	20.66	68	14.32	67	-74.85	66	-130.76
4	79	-15.69	78	70.21	77	-193.86	76	-75.51
MODEL #7								
1	37	-11.75	35	-31.04	33	-49.31	31	-62.34
2	57	-3.71	55	-32.21	53	-67.98	51	-91.60
3	69	22.23	68	13.84	67	-74.43	66	-127.63
4	79	-9.13	78	82.83	77	-166.20	76	-63.52
MODEL #8								
1	37	-13.98	35	-33.30	33	-50.51	31	-61.96
2	57	-7.91	55	-38.64	53	-74.77	51	-98.09
3	69	24.59	68	12.88	67	-74.08	66	-122.94
4	79	-.457	78	100.73	77	-123.81	76	-45.34

TABLE C-5

(Cont'd)

ROW	ELEM	τ	ELEM	τ	ELEM	τ	ELEM	τ
MODEL #9								
1	57	-23.02	55	-71.69	53	-114.47	51	-137.46
2	69	31.55	68	-25.76	67	-137.99	66	-160.25
3	79	12.09	78	193.23	77	115.96	76	34.66
MODEL #10								
1	57	.50	55	-32.80	53	-75.34	51	-103.76
2	69	17.65	68	4.98	67	-100.25	66	-165.02
3	79	-23.44	78	67.31	77	-235.27	76	-101.64
MODEL #11								
1	57	-3.05	55	-37.79	53	-80.08	51	-107.62
2	69	18.62	68	2.91	67	-102.21	66	-164.18
3	79	-16.65	78	81.15	77	-206.75	76	-90.12
MODEL #12								
1	57	-7.84	55	-44.69	53	-86.66	51	-112.99
2	69	20.07	68	-.60	67	-105.65	66	-163.01
3	79	-7.56	78	101.19	77	-162.31	76	-72.38

TABLE C-6

TRANSVERSE BENDING STRESS AT BOTTOM OF CROSS-STRUCTURE

MODEL HORIZONTALLY LOADED

LOAD: 99.4 lbs.

MODEL	NODE (ELEMENT)					
	6(85)	7(86)	8(77)	9(78)	10(79)	11(80)
1	-430.83	-614.96	-670.20	-1361.80	-968.19	-935.40
2	-347.79	-556.81	-760.09	-454.80	-364.15	-379.13
3	-354.99	-560.79	-743.19	-513.42	-434.36	-445.81
4	-366.08	-567.44	-736.14	-648.53	-535.11	-540.32
5	-511.33	-751.96	-831.76	-1752.30	-1300.92	-1274.48
6	-396.12	-646.10	-889.75	-533.28	-436.32	-455.55
7	-405.91	-645.51	-884.46	-629.54	-525.69	-542.18
8	-421.05	-667.75	-876.59	-779.46	-658.25	-668.89
9	-586.88	-892.18	-1004.90	-2186.69	-1682.65	-1667.55
10	-438.34	-729.03	-1013.87	-609.53	-505.97	-529.84
11	-450.16	-741.60	-1013.44	-725.36	-614.13	-636.76
12	-468.83	-761.70	-1013.09	-909.29	-781.36	-797.94

TABLE C-7

TRANSVERSE BENDING STRESS

COMBINED LOAD

MODEL #1

ROW	ELEM	σ	ELEM	σ	ELEM	σ	ELEM	σ
1	17	-191.77	15	-110.88	13	-54.77	11	-18.71
2	37	-483.40	35	-197.76	33	-136.69	31	-94.36
3	57	-152.15	55	-222.73	53	-162.27	51	-130.32
4	69	-65.54	68	-99.35	67	-124.06	66	-119.40
5	79T	-29.00	78T	-71.30	77T	-119.19	76	-138.50
6	79B	-108.72	78B	-227.50	77B	-242.86	86	-212.69

MODEL #2

1	18	-124.29	16	-74.74	14	-48.75	12	-31.51
2	37	-351.74	35	-134.98	33	-108.97	31	-80.61
3	57	-86.02	55	-166.10	53	-125.06	51	-107.09
4	69	-58.02	68	-83.72	67	-106.09	66	-95.80
5	79T	-54.48	78T	-71.03	77T	-82.53	76	-109.33
6	79B	-2.12	78B	-121.95	77B	-183.65	86	-143.62

MODEL #3

1	18	-140.96	16	-82.67	14	-52.84	12	-32.96
2	37	-366.46	35	-144.28	33	-114.67	31	-84.45
3	57	-94.90	55	-173.70	53	-130.79	51	-111.35
4	69	-60.49	68	-86.54	67	-108.84	66	-98.94
5	79T	-53.58	78T	-72.04	77T	-86.17	76	-111.71
6	79B	+3.30	78B	-130.24	77B	-185.41	86	-147.77

TABLE C-7

(Cont'd)

ROW	ELEM	σ	ELEM	σ	ELEM	σ	ELEM	σ
MODEL #4								
1	18	-162.50	16	-91.83	14	-56.96	12	-33.45
2	37	-387.04	35	-156.47	33	-121.59	31	-88.79
3	57	-106.73	55	-183.80	53	-138.14	51	-116.58
4	69	-63.11	68	-89.88	67	-112.30	66	-103.05
5	79T	-51.09	78T	-72.93	77T	-91.23	76	-115.32
6	79B	+13.87	78B	-142.37	77B	-190.23	86	-155.29
MODEL #5								
1	37	-366.32	35	-294.80	33	-211.45	31	-139.62
2	57	-623.03	55	-344.32	53	-239.05	51	-175.05
3	69	-80.37	68	-180.04	67	-148.69	66	-136.15
4	79T	96.50	78T	-5.90	77T	-89.27	76	-117.91
5	79B	+348.50	78B	-59.06	77B	-203.83	86	-185.19
MODEL #6								
1	38	-199.88	36	-137.74	34	-103.08	32	-77.37
2	57	-362.80	55	-193.75	53	-147.34	51	-112.55
3	69	-68.36	68	-148.34	67	-121.45	66	-108.52
4	79T	-13.37	78T	-53.90	77T	-86.82	76	-102.40
5	79B	+58.75	78B	-81.14	77B	-124.06	86	-110.80
MODEL #7								
1	38	-231.72	36	-158.03	34	-117.61	32	-87.25
2	57	-390.29	55	-212.64	53	-160.39	51	-122.23
3	69	-72.67	68	-153.56	67	-126.20	66	-113.16

TABLE C-7

(Cont'd)

MODEL #7 (Cont'd)

ROW	ELEM	σ	ELEM	σ	ELEM	σ	ELEM	σ
4	79T	-6.22	78T	-51.47	77T	-88.18	76	-104.10
5	79B	+78.94	78B	-79.43	77B	-126.94	86	-115.16
MODEL #8								
1	38	-275.53	36	-185.27	34	-136.97	32	-99.73
2	57	-429.71	55	-238.73	53	-177.77	51	-134.78
3	69	-77.41	68	-160.04	67	-132.18	66	-119.05
4	79T	6.37	78T	-46.71	77T	-89.42	76	-106.45
5	79B	+112.61	78B	-75.75	77B	-133.90	86	-123.20
MODEL #9								
1	57	-901.69	55	-613.51	53	-419.05	51	-295.88
2	69	-370.51	68	-242.05	67	-212.23	66	-177.70
3	79T	268.92	78T	119.08	77T	-34.81	76	-96.05
4	79B	+642.12	78B	+181.86	78B	-150.05	86	-138.64
MODEL #10								
1	58	-306.41	56	-218.83	54	-163.56	52	-125.62
2	69	-291.12	68	-163.70	67	-143.22	66	-115.34
3	79T	62.28	78T	-85.83	77T	-73.91	76	-93.77
4	79B	+123.76	78B	-32.51	77B	-63.85	86	-70.91
MODEL #11								
1	58	-363.78	56	-257.24	54	-190.99	52	-145.24
2	69	-302.71	68	-174.73	67	-152.73	66	-124.02
3	79T	75.15	78T	-80.82	77T	-73.52	76	-95.37
4	79B	+160.63	78B	-18.38	77B	-66.84	86	-74.87

TABLE C-7

(Cont'd)

MODEL #12

ROW	ELEM	σ	ELEM	σ	ELEM	σ	ELEM	σ
1	58	-449.07	56	-313.92	54	-229.96	52	-172.21
2	69	-317.96	68	-189.38	67	-165.44	66	-135.59
3	79T	97.66	78T	-71.26	77T	-71.29	76	-97.08
4	79B	+221.46	78B	+5.90	77B	-68.81	86	-82.06

σ: psi

T: Top of Element

B: Bottom of Element

TABLE C-8

SHEAR STRESS

COMBINED LOAD

MODEL #1

ROW	ELEM	τ	ELEM	τ	ELEM	τ	ELEM	τ
1	17	72.45	15	47.47	13	34.72	11	29.10
2	37	279.25	35	126.11	33	97.04	31	77.93
3	57	191.59	55	195.95	53	157.36	51	128.36
4	69	137.26	68	191.42	67	174.68	66	141.78
5	79	48.29	78	142.32	77	164.39	76	142.36

MODEL #2

1	17	117.59	15	82.34	13	62.09	11	52.43
2	37	258.47	35	123.24	33	48.26	31	80.05
3	57	164.62	55	167.04	53	133.55	51	110.67
4	69	124.24	68	169.88	67	139.26	66	105.42
5	79	77.15	78	183.92	77	73.54	76	104.67

MODEL #3

1	17	113.13	15	78.10	13	58.35	11	49.11
2	37	259.64	35	123.16	33	97.75	31	79.39
3	57	166.74	55	169.50	53	135.77	51	112.46
4	69	125.54	68	172.06	67	143.20	66	109.65
5	79	75.67	78	181.40	77	83.47	76	109.01

MODEL #4

1	17	106.60	15	72.20	13	53.31	11	44.69
2	37	261.73	35	123.29	33	97.21	31	78.65
3	57	170.10	55	173.32	53	139.13	51	115.10

TABLE C-8

(Cont'd)

MODEL #4 (Cont'd)

ROW	ELEM	τ	ELEM	τ	ELEM	τ	ELEM	τ
4	69	127.40	68	175.20	67	148.80	66	115.53
5	79	72.81	78	176.83	77	97.44	76	114.98
MODEL #5								
1	37	30.83	35	45.40	33	41.99	31	38.76
2	57	278.09	55	197.66	53	163.98	51	134.11
3	69	215.42	68	268.14	67	215.20	66	170.91
4	79	71.44	78	173.37	77	189.89	76	159.30
MODEL #6								
1	37	109.63	35	95.56	33	80.20	31	73.60
2	57	244.19	55	172.69	53	142.98	51	118.07
3	69	188.05	68	229.19	67	168.73	66	130.58
4	79	111.20	78	233.28	77	114.90	76	128.39
MODEL #7								
1	37	102.96	35	89.94	33	75.44	31	69.29
2	57	246.58	55	174.75	53	144.72	51	119.40
3	69	190.42	68	232.73	67	173.72	66	135.33
4	79	108.81	78	229.24	77	123.88	76	132.41
MODEL #8								
1	37	92.83	35	81.87	33	68.81	31	63.31
2	57	250.50	55	178.05	53	147.47	51	121.47
3	69	194.02	68	238.05	67	180.92	66	141.93
4	79	104.52	78	222.34	77	136.15	76	137.76

TABLE C-8

(Cont'd)

MODEL #9

ROW	ELEM	τ	ELEM	τ	ELEM	τ	ELEM	τ
1	57	203.55	55	178.33	53	151.31	51	125.91
2	69	346.13	68	305.94	67	262.83	66	205.51
3	79	103.50	78	210.50	77	204.16	76	177.76

MODEL #10

1	57	204.29	55	173.48	53	147.55	51	126.78
2	69	304.48	68	250.53	67	196.26	66	152.72
3	79	153.95	78	290.71	77	145.82	76	150.02

MODEL #11

1	57	203.76	55	173.36	53	147.43	51	126.34
2	69	307.98	68	255.20	67	202.50	66	158.34
3	79	150.76	78	285.14	77	154.11	76	154.01

MODEL #12

1	57	203.20	55	173.48	53	147.49	51	125.85
2	69	313.38	68	262.40	67	211.91	66	166.39
3	79	145.18	78	275.79	77	165.04	76	159.24

TABLE C-9

TRANSVERSE BENDING STRESS AT BOTTOM OF CROSS-STRUCTURE

COMBINED LOAD

MODEL	NODE (ELEMENT)					
	6(85)	7(86)	8(77)	9(78).	10(79)	11(80)
1	-171.74	-212.69	-242.86	-227.50	108.72	192.62
2	-117.54	-143.62	-183.65	-121.95	-2.12	17.44
3	-121.46	-147.77	-185.41	-130.24	+3.30	+29.84
4	-127.94	-155.29	-190.23	-142.37	+13.87	+51.05
5	-158.21	-185.19	-203.83	-59.06	+348.78	+479.40
6	-104.16	-110.80	-124.06	-81.14	+58.75	+90.51
7	-108.08	-115.61	-126.94	-79.43	+78.94	+120.42
8	-114.60	-123.20	-133.90	-75.75	+112.61	+169.04
9	-136.41	-138.64	-150.05	+181.86	+642.12	857.10
10	-87.47	-70.91	-63.85	-32.51	123.76	173.31
11	-91.25	-74.87	-66.84	-18.38	160.63	224.44
12	-97.34	-82.06	-68.81	5.90	221.46	307.21

TABLE C-10

FRINGE ORDERS AT CROSS-STRUCTURE BOTTOM

VERTICAL LOAD

LOAD: 99.4 lbs.

	NODE					
MODEL	6	7	8	9	10	11
1	2.1	2.6	3.5	5.6	6.2	6.8
2	2.51	2.9	3.0	2.8	2.7	2.4
3	2.52	3.0	2.6	3.0	3.0	3.0
4	2.58	3.0	2.5	2.8	3.0	3.1
5	3.1	3.9	5.5	8.5	10	10.2
6	3.0	2.9	3.9	3.75	3.60	3.30
7	3.23	4.0	3.7	4.14	4.0	3.8
8	3.0	3.9	3.5	3.8	4.0	4.1
9	3.95	5.0	8	12	14	15.75
10	3.36	4.29	4.0	3.9	4.0	3.9
11	3.55	4.8	3.6	4.3	4.66	4.66
12	3.52	4.8	4.1	5.0	5.30	5.40

TABLE C-11

FRINGE ORDERS AT CROSS-STRUCTURE BOTTOM

HORIZONTAL LOAD

LOAD: 99.4 lbs.

MODEL	NODE 6	7	8	9	10	11
1	3.9	5.4	9	6.9	6.9	6.7
2	2.8	3.2	1	3.0	2.9	2.8
3	2.7	3.3	2	3.5	2.9	2.9
4	2.9	3.8	2	3.5	3.4	3.4
5	4.3	6.2	11	9.5	9.0	8.8
6	3.1	4.0	2	3.5	3.1	2.9
7	2.9	3.9	2	3.6	3.0	2.9
8	3.1	4.2	2	4.1	3.9	3.9
9	5.0	7.2	13	11.5	11.1	11.0
10	3.1	4.2	2	3.4	3.2	3.0
11	3.3	4.9	2	3.8	3.6	3.4
12	3.5	5	2	4.5	4.2	4.2

TABLE C-12

FRINGE ORDERS AT CROSS-STRUCTURE BOTTOM

VERTICAL LOAD - TOP STIFFENING ONLY

LOAD: 99.4 lbs.

	NODE					
MODEL	6	7	8	9	10	11
2	1.9	2	3	3.5	3.9	4.0
3	2.0	2.1	3.5	4.2	5.1	5
4	2.0	2.1	4	4.5	5	5.3
6	2.2	2.8	4	6	7	7.9
7	2.4	2.9	5	6.4	7.2	7.4
8	2.6	2.9	6	7.1	7.9	8.0
10	2.9	3.2	5	7.8	9	10
11	3.0	3.8	7	8.5	10.1	11
12	3.2	4.0	8	9.3	10.9	11.1

TABLE C-13

FRINGE ORDERS AT CROSS-STRUCTURE BOTTOM

HORIZONTAL LOAD - TOP STIFFENING ONLY

LOAD: 99.4 lbs.

	NODE					
MODEL	6	7	8	9	10	11
2	2.9	4.1	7	5.2	4.9	4.9
3	2.9	4.0	8	5.5	5.1	5.0
4	3.0	4.4	8	5.9	5.5	5.5
6	3.3	4.9	9	7	6.4	6.2
7	3.4	4.9	10	6.9	6.5	6.2
8	3.6	5.0	10	7.5	6.8	6.5
10	3.8	5.1	11	7.9	7.5	7.4
11	4.2	6.3	12	9.1	8.9	8.8
12	4.4	6.5	13	9.9	9.4	9.2

APPENDIX D

ORIGINAL DATA

Sample Computer Input

Illustrated in Figure D-1 is the finite element grid used for this thesis. The initial size or fineness of the mesh is rather arbitrary since it can be reduced on subsequent runs to provide the desired accuracy. For the computations in this thesis, only one grid was used because of time and monetary considerations. Regardless of initial overall size of the mesh, smaller elements should be used in regions of suspected stress concentrations. As can be seen in the figure, the elements are smaller in the area of the junction of hull and cross-structure. The small arrows on the figure are the points of applied load.

Following Figure D-1, the entire input deck for model number four is listed as an example for anyone having occasion to use the FINEL program. The comments printed with the listing refer to the subdivisions of the input deck as listed in the User's Manual, Reference (14).

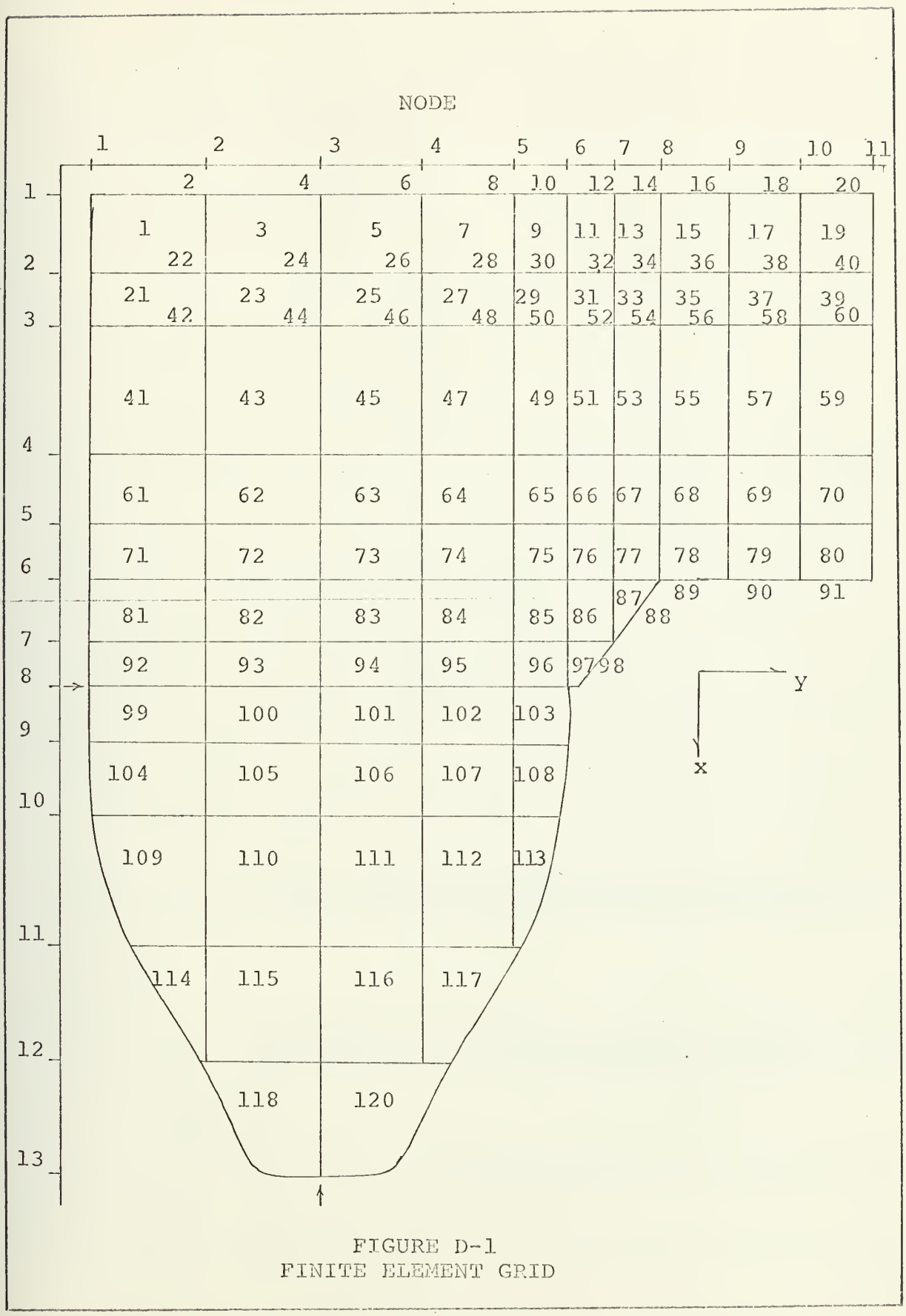

FIGURE D-1
FINITE ELEMENT GRID

```
C  INITIAL CARDS (SAMPLE INPUT IS FOR MODEL NUMBER 4)
     4   13    2    1    2            POUNDS      INCHES
     1    3    4
  11 11 11 11 11 11  7  6  6  6  5  5  3
C  MATERIAL CHARACTERISTICS
     1  3400000.0        .38
C  ELEMENT PROPERTIES
     1       .250
     2       .094
C  NODE COORDINATES
     1    1        0.0         0.0
     1    2        0.0         0.9
     1    3        0.0         1.7
     1    4        0.0         2.4
     1    5        0.0         3.0
     1    6        0.0         3.4
     1    7        0.0         3.7
     1    8        0.0         4.0
     1    9        0.0         4.5
     1   10        0.0         5.0
     1   11        0.0        5.47
     2    1       0.54         0.0
     2    2       0.54         0.9
     2    3       0.54         1.7
     2    4       0.54         2.4
     2    5       0.54         3.0
     2    6       0.54         3.4
     2    7       0.54         3.7
     2    8       0.54         4.0
     2    9       0.54         4.5
     2   10       0.54         5.0
     2   11       0.54        5.47
     3    1        0.9         0.0
     3    2        0.9         0.9
     3    3        0.9         1.7
     3    4        0.9         2.4
```

3	5	0.9	3.0
3	6	0.9	3.4
3	7	0.9	3.7
3	8	0.9	4.0
3	9	0.9	4.5
3	10	0.9	5.0
3	11	0.9	5.47
4	1	1.8	0.0
4	2	1.8	0.9
4	3	1.8	1.7
4	4	1.8	2.4
4	5	1.8	3.0
4	6	1.8	3.4
4	7	1.8	3.7
4	8	1.8	4.0
4	9	1.8	4.5
4	10	1.8	5.0
4	11	1.8	5.47
5	1	2.3	0.0
5	2	2.3	0.9
5	3	2.3	1.7
5	4	2.3	2.4
5	5	2.3	3.0
5	6	2.3	3.4
5	7	2.3	3.7
5	8	2.3	4.0
5	9	2.3	4.5
5	10	2.3	5.0
5	11	2.3	5.47
6	1	2.7	0.0
6	2	2.7	0.9
6	3	2.7	1.7
6	4	2.7	2.4
6	5	2.7	3.0
6	6	2.7	3.4
6	7	2.7	3.7

6	8	2.7	4.0
6	9	2.7	4.5
6	10	2.7	5.0
6	11	2.7	5.47
7	1	3.1	0.0
7	2	3.1	0.9
7	3	3.1	1.7
7	4	3.1	2.4
7	5	3.1	3.0
7	6	3.1	3.4
7	7	3.1	3.7
8	1	3.42	0.0
8	2	3.42	0.9
8	3	3.42	1.7
8	4	3.42	2.4
8	5	3.42	3.0
8	6	3.42	3.4
9	1	3.8	0.0
9	2	3.8	0.9
9	3	3.8	1.7
9	4	3.8	2.4
9	5	3.8	3.0
9	6	3.8	3.4
10	1	4.3	0.0
10	2	4.3	0.9
10	3	4.3	1.7
10	4	4.3	2.4
10	5	4.3	3.0
10	6	4.3	3.3
11	1	5.2	.28
11	2	5.2	0.9
11	3	5.2	1.7
11	4	5.2	2.4
11	5	5.2	3.0
12	1	6.9	.75
12	2	6.9	0.9

```
    12     3        6.0        1.7
    12     4        6.0        2.4
    12     5        6.0       2.55
    13     1       6.84        1.2
    13     2       6.84        1.7
    13     3       6.84        2.1
C MEMBER DATA
     1   6       1  3        1   1   2   1   1   2   2   2
     2   5       2  3        1   1   1   2  -1
     3   6       1  3        1   2   2   2   1   3   2   3
     4   5       2  3        1   2   1   3  -1
     5   6       1  3        1   3   2   3   1   4   2   4
     6   5       2  3        1   3   1   4  -1
     7   6       1  3        1   4   2   4   1   5   2   5
     8   5       2  3        1   4   1   5  -1
     9   6       1  3        1   5   2   5   1   6   2   6
    10   5       2  3        1   5   1   6  -1
    11   6       1  3        1   6   2   6   1   7   2   7
    12   5       2  3        1   6   1   7  -1
    13   6       1  3        1   7   2   7   1   8   2   8
    14   5       2  3        1   7   1   8  -1
    15   6       1  3        1   8   2   8   1   9   2   9
    16   5       2  3        1   8   1   9  -1
    17   6       1  3        1   9   2   9   1  10   2  10
    18   5       2  3        1   9   1  10  -1
    19   6       1  3        1  10   2  10   1  11   2  11
    20   5       2  3        1  10   1  11  -1
    21   6       1  3        2   1   3   1   2   2   3   2
    23   6       1  3        2   2   3   2   2   3   3   3
    25   6       1  3        2   3   3   3   2   4   3   4
    27   6       1  3        2   4   3   4   2   5   3   5
    29   6       1  3        2   5   3   5   2   6   3   6
    31   6       1  3        2   6   3   6   2   7   3   7
    33   6       1  3        2   7   3   7   2   8   3   8
    35   6       1  3        2   8   3   8   2   9   3   9
    37   6       1  3        2   9   3   9   2  10   3  10
```

39	6	1	3	2	10	3	10	2	11	3	11
41	6	1	3	3	1	4	1	3	2	4	2
43	6	1	3	3	2	4	2	3	3	4	3
45	6	1	3	3	3	4	3	3	4	4	4
47	6	1	3	3	4	4	4	3	5	4	5
49	6	1	3	3	5	4	5	3	6	4	6
51	6	1	3	3	6	4	6	3	7	4	7
53	6	1	3	3	7	4	7	3	8	4	8
55	6	1	3	3	8	4	8	3	9	4	9
57	6	1	3	3	9	4	9	3	10	4	10
59	6	1	3	3	10	4	10	3	11	4	11
61	6	1	3	4	1	5	1	4	2	5	2
62	6	1	3	4	2	5	2	4	3	5	3
63	6	1	3	4	3	5	3	4	4	5	4
64	6	1	3	4	4	5	4	4	5	5	5
65	6	1	3	4	5	5	5	4	6	5	6
66	6	1	3	4	6	5	6	4	7	5	7
67	6	1	3	4	7	5	7	4	8	5	8
68	6	1	3	4	8	5	8	4	9	5	9
69	6	1	3	4	9	5	9	4	10	5	10
70	6	1	3	4	10	5	10	4	11	5	11
71	6	1	3	5	1	6	1	5	2	6	2
72	6	1	3	5	2	6	2	5	3	6	3
73	6	1	3	5	3	6	3	5	4	6	4
74	6	1	3	5	4	6	4	5	5	6	5
75	6	1	3	5	5	6	5	5	6	6	6
76	6	1	3	5	6	6	6	5	7	6	7
77	6	1	3	5	7	6	7	5	8	6	8
78	6	1	3	5	8	6	8	5	9	6	9
79	6	1	3	5	9	6	9	5	10	6	10
80	6	1	3	5	10	6	10	5	11	6	11
81	6	1	3	6	1	7	1	6	2	7	2
82	6	1	3	6	2	7	2	6	3	7	3
83	6	1	3	6	3	7	3	6	4	7	4
84	6	1	3	6	4	7	4	6	5	7	5
85	6	1	3	6	5	7	5	6	6	7	6

```
  96  6     1 3       6  6  7  6  6  7  7  7
  97  1     1 3       6  8  7  7  6  7
  98  5     2 3       6  8  7  7
  89  5     2 3       6  8  6  9 -1
  90  5     2 3       6  9  6 10
  91  5     2 3       6 10  6 11
  92  6     1 3       7  1  8  1  7  2  8  2
  93  6     1 3       7  2  8  2  7  3  8  3
  94  6     1 3       7  3  8  3  7  4  8  4
  95  6     1 3       7  4  8  4  7  5  8  5
  96  6     1 3       7  5  8  5  7  6  8  6
  97  1     1 3       7  7  8  6  7  6
  98  5     2 3       7  7  8  6
  99  6     1 3       8  1  9  1  8  2  9  2
 100  6     1 3       8  2  9  2  8  3  9  3
 101  6     1 3       8  3  9  3  8  4  9  4
 102  6     1 3       8  4  9  4  8  5  9  5
 103  6     1 3       8  5  9  5  8  6  9  6
 104  6     1 3       9  1 10  1  9  2 10  2
 105  6     1 3       9  2 10  2  9  3 10  3
 106  6     1 3       9  3 10  3  9  4 10  4
 107  6     1 3       9  4 10  4  9  5 10  5
 108  2     1 3       9  5 10  5  9  6 10  6
 109  2     1 3      10  1 11  1 10  2 11  2
 110  6     1 3      10  2 11  2 10  3 11  3
 111  6     1 3      10  3 11  3 10  4 11  4
 112  6     1 3      10  4 11  4 10  5 11  5
 113  1     1 3      10  5 11  5 10  6
 114  2     1 3      11  1 12  1 11  2 12  2
 115  6     1 3      11  2 12  2 11  3 12  3
 116  6     1 3      11  3 12  3 11  4 12  4
 117  2     1 3      11  4 12  4 11  5 12  5
 118  2     1 3      12  1 13  1 12  3 13  2
 120  2     1 3      12  3 13  2 12  5 13  3
                     15
C BOUNDARY CONDITIONS
```

```
     1    11     11
     2    11     01
     3    11     01
     4    11     01
     5    11     01
     6    11     01
    15
C NODE FORCES
   3
     1    13     2      -99.4
     2     9     1                    99.4
     3    13     2      -99.4
     3     9     1                    99.4
          15
C EXIT CONTROL
   1
```

Fringe Pattern Photographs

The following figures present the fringe pattern photographs for all models and all loadings. The sequence of the figures is such that the first four photographs are for the first four models with parameters as listed in Table B-1. The next three photographs are for models of a particular B/D grouping, however, they are stiffened along the top edge only. This sequence is repeated for each B/D group and for each type of loading. The first six figures are for the vertical loads, while the remaining six are for the horizontal loads.

MODEL 1

MODEL 2

MODEL 3

MODEL 4

FIGURE D-2
FRINGE PATTERNS, B/D=4.0, VERTICAL LOAD

MODEL 2

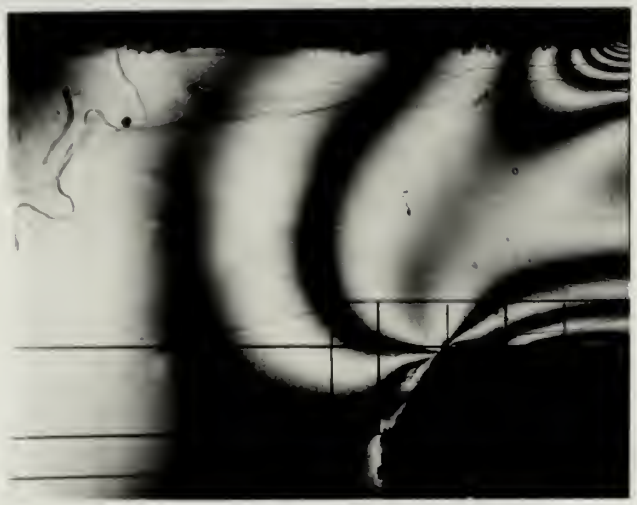

MODEL 3

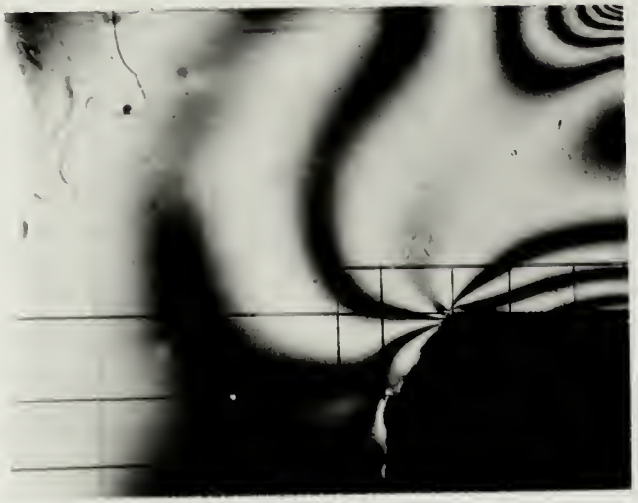

MODEL 4

FIGURE D-3, FRINGE PATTERNS, B/D = 4.0, VERTICAL LOAD, TOP STIFFENING ONLY

MODEL 5

MODEL 6

MODEL 7

MODEL 8

FIGURE D-4
FRINGE PATTERNS, B/D = 5.0, VERTICAL LOAD

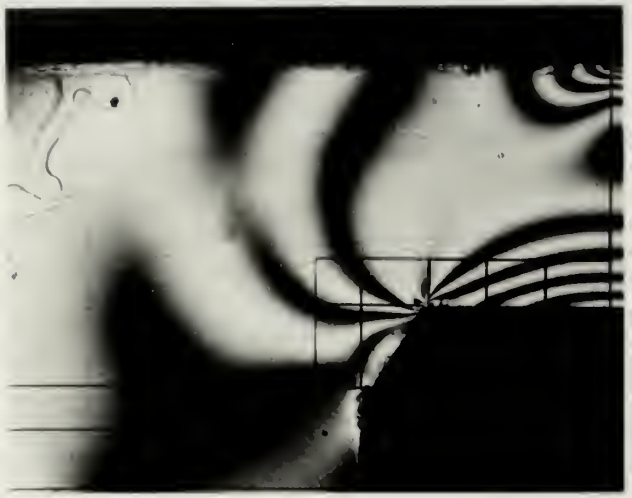

MODEL 6

MODEL 7

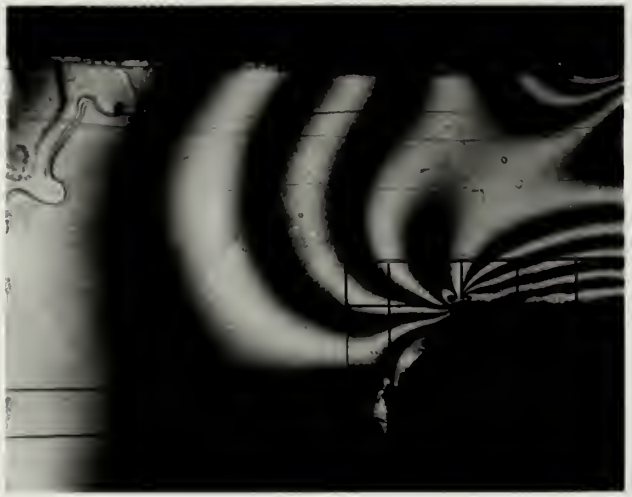

MODEL 8

FIGURE D-5, FRINGE PATTERNS, B/D = 5.0, VERTICAL LOAD, TOP STIFFENING ONLY

MODEL 9

MODEL 10

MODEL 11

MODEL 12

FIGURE D-6
FRINGE PATTERNS B/D = 6.0, VERTICAL LOAD

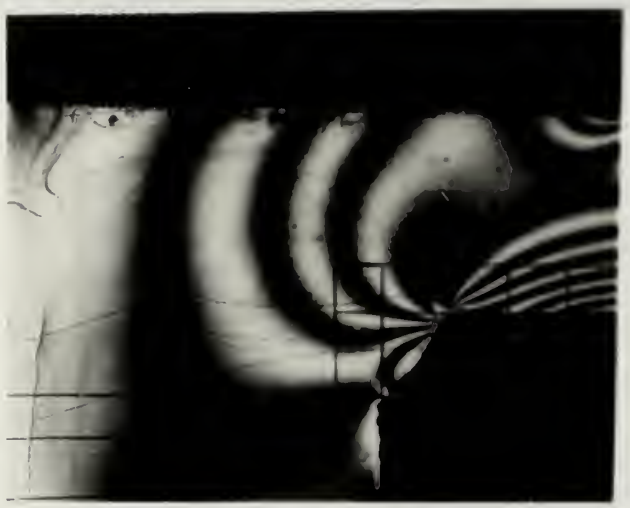

MODEL 10

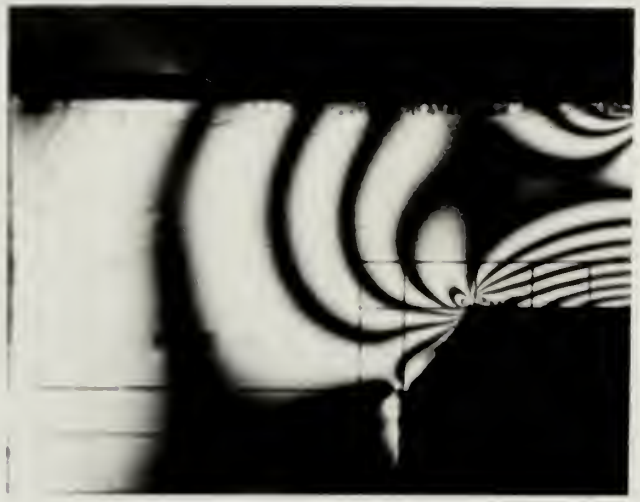

MODEL 11

MODEL 12

FIGURE D-7, FRINGE PATTERNS, B/D = 6.0, VERTICAL LOAD, TOP STIFFENING ONLY

MODEL 1

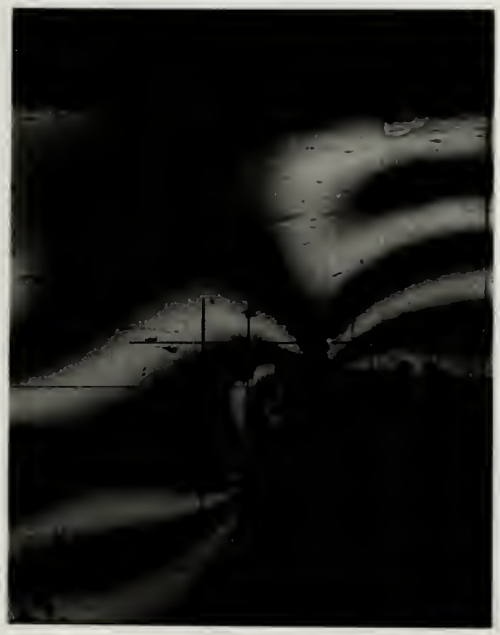

MODEL 2

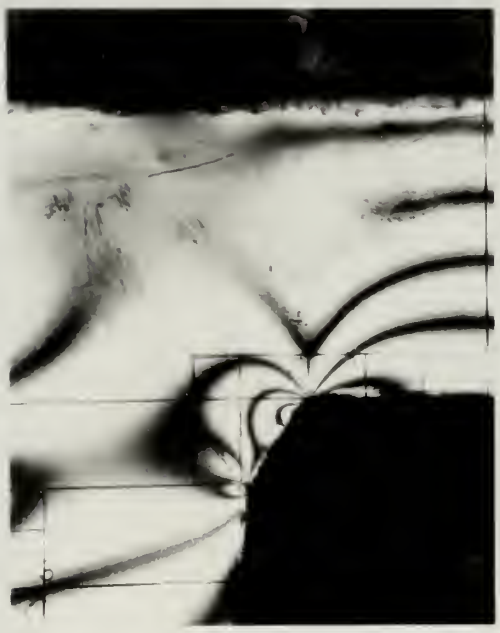

MODEL 3

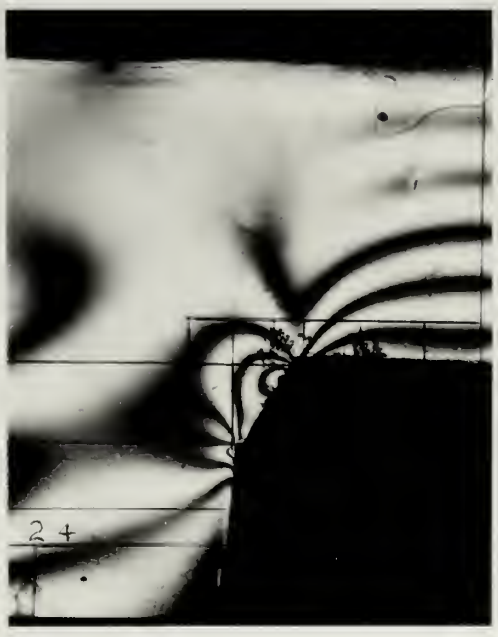

MODEL 4

FIGURE D-8

FRINGE PATTERNS, B/D =4.0, HORIZONTAL LOAD

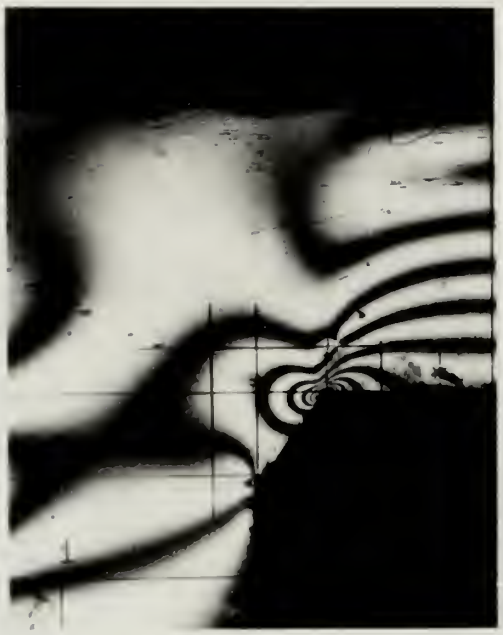

MODEL 2

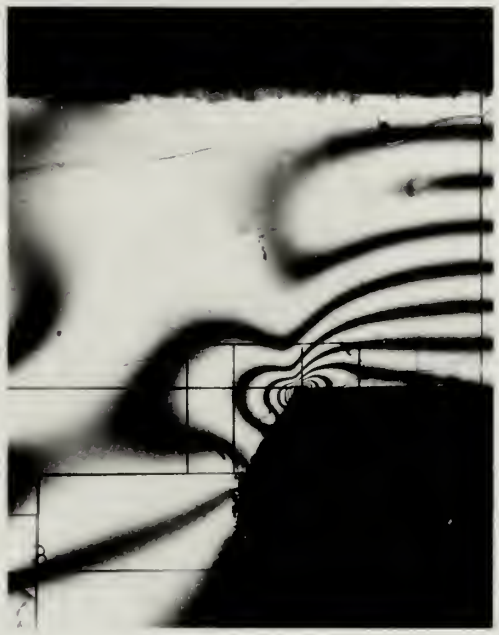

MODEL 3

MODEL 4

FIGURE D-9

FRINGE PATTERNS, B/D = 4.0, HORIZONTAL LOAD

TOP STIFFENING ONLY

MODEL 5

MODEL 6

MODEL 7

MODEL 8

FIGURE D-10

FRINGE PATTERNS, B/D = 5.0, HORIZONTAL LOAD

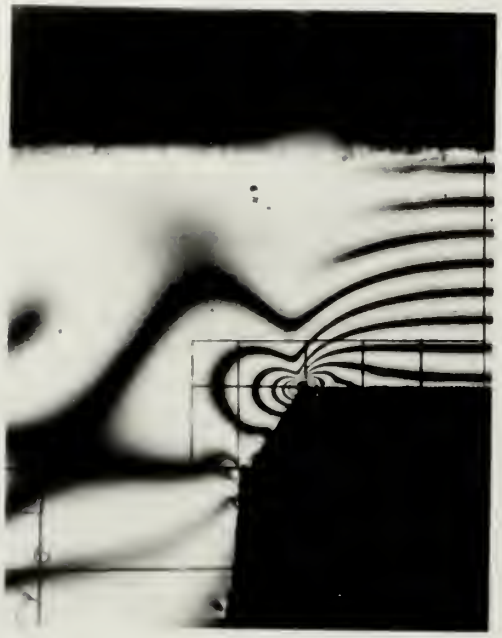

MODEL 6

MODEL 7

MODEL 8

FIGURE D-11

FRINGE PATTERNS, B/D = 5.0, HORIZONTAL LOAD

TOP STIFFENING ONLY

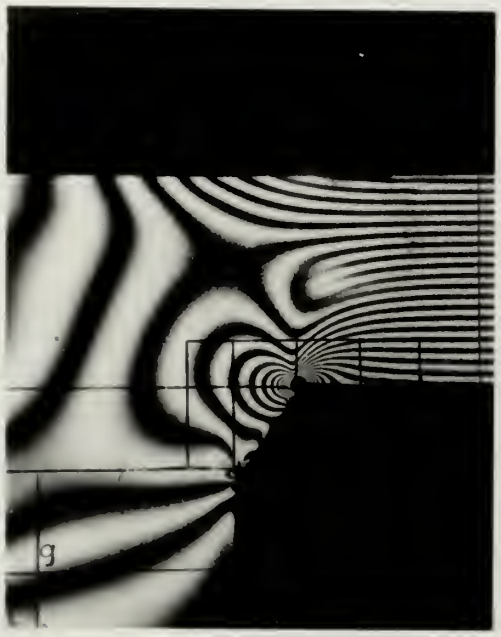

MODEL 9

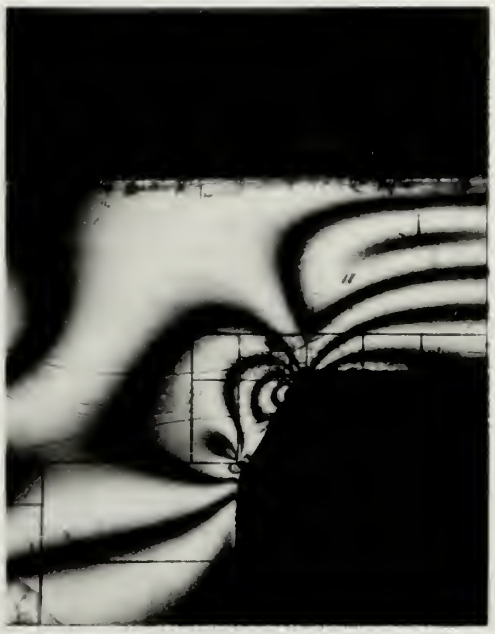

MODEL 10

MODEL 11

MODEL 12

FIGURE D-12
FRINGE PATTERNS, B/D = 6.0, HORIZONTAL LOAD

MODEL 10

MODEL 11

MODEL 12

FIGURE D-13

FRINGE PATTERNS, B/D = 6.0, HORIZONTAL LOAD

TOP STIFFENING ONLY

APPENDIX E

REFERENCES

1. Ballentine, J. C., "Photoelastic Study of Interrupted Pressure Vessel Frames," Thesis, Department of Naval Architecture and Marine Engineering, M.I.T., 1967.

2. Brand, L. and Tolefson, D. C., "Introduction to Finite Element Methods of Structural Analysis," Marine Technology, Vol. 5, #4, October 1968.

3. Christensen, J. E., "The New Catamaran Submarine Rescue Ships: ASR 21 Class," Marine Technology, Vol. 7, #3, July 1970.

4. Dally, James W., Experimental Stress Analysis, McGraw-Hill, New York, 1965.

5. Dinsenbacher, A., "Sea Loads on Catamaran Cross-Structure: Model Test Preliminary Results," David Taylor Model Basin, March 1966.

6. Hendry, A. W., Photoelastic Analysis, Pergamon Press, London, 1966.

7. Hendry, A. W., Elements of Experimental Stress Analysis, McMillan Co., New York, 1964.

8. Hetenyi, M., Handbook of Experimental Stress Analysis, John Wiley & Sons, Inc., New York, 1963.

9. Lankford, B. W., "The Structural Design of ASR Catamaran Cross-Structure," Naval Engineer's Journal, August 1967.

10. Maclaren, R. E., "Photoelastic Study of a Discontinuous Beam under Bending Load," Thesis, Department of Naval Architecture and Marine Engineering, M.I.T., 1966.

11. Miller, E. A., "A Photoelastic Analysis of Stress Distribution in Flat Plate Panels Simulating Ship Bulkheads," Thesis, Department of Naval Architecture and Marine Engineering, M.I.T., 1957.

12. Paulling, J. R., "The Analysis of Complex Ship Structures by the Finite Element Technique," Journal of Ship Research, Vol. 8, No. 3, December 1964.

13. Zienkiewcicz, O. C. and Cheung, Y. K., The Finite Element Method in Structural and Continuum Mechanics, McGraw-Hill Publishing Co., Ltd., London, 1967.

14. "Instructions for Use of the Modified Finite Element Program FINEL," Naval Ship Research and Development Center, Washington, D. C., August 1970.

15. Photolastic, Inc., Bulletin P1120, "Materials for Photoelastic Coatings and Photoelastic Models."

16. Submarine Rescue Ship ASR 21, Scantlings, Typical Sections, NavShips Drawing No. 800-2640547, Rev. A.

17. Photolastic, Inc., Bulletin 1B-P-330R, "Instructions for Making Photoelastic Models."

18. Holman, R., "A Photoelastic Study of the Stress Distribution in Stiffened Plating," Thesis, Department of Naval Architecture and Marine Engineering, M.I.T., 1955.

19. Chow, L., Conwam, H. D. and Winter, G., "Stresses in Deep Beams," A.S.C.E. Transactions, 1953, pp. 686-702.

Thesis 127308
M2513 Maclin
An investigation of stress distribution in a catamaran cross-structure.